CALCULATIONS of the ELECTRON ENERGY DISTRIBUTION FUNCTION in a URANIUM PLASMA by ANALYTIC and MONTE CARLO TECHNIQUES

by

CHARLES GARY BATHKE

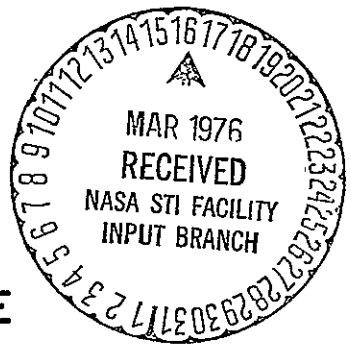

NUCLEAR ENGINEERING PROGRAM

UNIVERSITY of ILLINOIS at URBANA-CHAMPAIGN

URBANA, 1976

CALCULATIONS OF THE ELECTRON ENERGY DISTRIBUTION FUNCTION IN A URANIUM PLASMA BY ANALYTIC AND MONTE CARLO TECHNIQUES

BY

CHARLES GARY BATHKE

B.S., Ohio State University, 1970
M.S., University of Illinois, 1972

THESIS

Submitted in partial fulfillment of the requirements
for the degree of Doctor of Philosophy in Nuclear Engineering
in the Graduate College of the
University of Illinois at Urbana-Champaign, 1976

Urbana, Illinois

ABSTRACT

Electron energy distribution functions have been calculated in a U^{235}-plasma at 1 atmosphere for various plasma temperatures (5000-8000°K) and neutron fluxes (2×10^{16}-2×10^{12} neutrons/(cm^3-sec)). The distributions are assumed to be a summation of a high-energy tail and a Maxwellian distribution. The sources of energetic electrons considered are the fission-fragment induced ionization of uranium and the electron induced ionization of uranium. The calculation of the high-energy tail is reduced to an electron slowing down calculation, from the most energetic source (~ 2.1 keV) to the energy where the electron is assumed to be incorporated into the Maxwellian distribution (~ 15 eV). The pertinent collisional processes are electron-electron scattering and electron induced ionization and excitation of uranium.

Two distinct methods have been employed in the calculation of the distributions. One method is based upon the assumption of continuous slowing and yields a distribution inversely proportional to the stopping power. An iteration scheme is utilized to include the secondary electron avalanche.

In the other method, a governing equation is derived without assuming continuous electron slowing. This equation is solved by a Monte Carlo technique which simulates Coulombic collisional slowing analytically while ionization and excitation events are simulated in a random walk fashion. Consequently, the secondary electron avalanche is included explicitly.

Both methods yield comparable results at high energies ($\gtrsim$ 100 eV), with disparities arising at lower energies due to the inapplicability of the continuous slowing assumption. The distribution functions calculated

in both models are observed to be linearly dependent upon the neutron flux while inversely proportional to the plasma temperature. The electrons within the calculated high-energy tail induce $\sim 10^{14}$ more excitations of uranium per cm^3 per second than are induced by Maxwellian electrons. Since the threshold of non-Maxwellian behavior is ~ 15 eV, the present results suggest seeding the plasma with a species having a high excitation threshold, e.g. helium, in order to better capitalize upon the excitation characteristics of the high-energy tail in possible applications as a lasing medium or a radiation source.

ACKNOWLEDGMENT

The author wishes to express sincere gratitude to Professor George H. Miley, his advisor, without whose guidance and invaluable suggestions the present work would not have been possible.

The author also wishes to thank his thesis committee, especially Professor M. Raether and Professor A. B. Chilton for their valuable discussions on various aspects of the thesis. Many of the author's colleagues, Dr. R. H. Lo, Dr. B. H. Wang, R. Miller, E. Maceda, and Dr. Chan Choi, to name a few, provided beneficial criticism and helpful suggestions which expedited the completion of this work.

The author is appreciative of the crucial background information made available by Dr. K. H. Thom and Dr. Frank Hohl. In addition, the author is grateful for the financial support for this work provided by the NASA-AEC Space Power Office under Grant US NASA NSG 1063.

The author wants to express appreciation for the morale support provided by his parents, early mentor Mr. John Clark, and his wife, Cynthia, who also aided in the proofreading of the final manuscript.

The author thanks Ms. Jeri Borchers for the excellent typing of the thesis manuscript.

TABLE OF CONTENTS

Page

Page

CHAPTER I

INTRODUCTION

A. Definition of Problem

The objective of this study is the deduction of the effect of the presence of fission-fragments upon the electron energy distribution function in a uranium plasma. Parametric studies of the neutron-flux (a measure of the fission-fragment density) and temperature dependence of the distribution function are undertaken to provide insight into the plasma conditions under which the fission-fragments have the most pronounced effect upon the distribution function. These calculations will be obtained by two separate models; a simple model for survey calculations and a second, more refined model, by which the accuracy of the former may be judged.

Primary emphasis is placed upon the high-energy tail of the distribution function, i.e., at energies above the excitation threshold, as it is anticipated that the results generated herein will be used for the calculation of excitation rates. At such energies, the calculation of the distribution function reduces to the problem of slowing down from a source. The source of electrons to be considered here is comprised of two distinct components, each distributed in energy. The first consists of those electrons generated by the fission-fragment induced ionization of the background uranium during their slowing down process, while the second consists of those secondary electrons produced through the ionization of uranium by energetic electrons as they thermalize.

B. Motivation

The motivating forces behind this study can best be identified by examining some of the anticipated applications of a uranium plasma. Historically, the first application envisioned was the utilization of the plasma as an energy source for an ion rocket engine termed the nuclear light-bulb concept.[1-4] The success of the idea depends upon the efficiency at which the energy released during the fissioning of uranium is transmitted to and absorbed by the hydrogen fuel. The energy transmission process consists of a conduction chain and a radiation chain. In the conduction chain, the energy deposited within the plasma by the neutrons and fission-fragments is conducted away from its source to the hydrogen fuel. In the radiation chain, a portion of the fission-fragment energy is transmitted to electrons through the ionization of the background uranium. The electrons in turn excite the background which transforms the energy into radiation as the atoms de-excite. Then both the line radiation and the blackbody radiation pass through a "window" into the fuel where it is to be absorbed.

Two additional applications make extensive use of the radiation chain, namely direct nuclear pumping[5-6] and photo-chemical production[7] by extracting energy from the uranium plasma in the form of light. In the scheme of direct nuclear pumping, a population inversion is sought either by seeking a situation where the uranium will lase or by transferring the energy from the uranium plasma to a second species which would lase. In the latter scheme, less stringent requirements are placed upon the excitation rates, as a population inversion of the uranium itself is unnecessary.

The success of this scheme depends solely upon the ability to shape the radiation spectrum via either the determination of the plasma opacity or the transluscent properties of the "window".

A fourth application involves the high efficiency extraction of energy from the uranium plasma through an MHD cycle.[8] This scheme may be combined with either of the two previous schemes which would serve as topping cycles to further enhance efficiency.

From these possible applications, the importance of the calculation of the electron energy distribution function can be gauged. The success of most of these schemes depends upon an accurate determination of the excitation rates. A prime means of exciting atoms is through electron induced excitation. Consequently, at the heart of the problem is the need for a detailed knowledge of the number of electrons capable of inducing excitation. Such a query can be satisfied only with a detailed calculation of the electron energy distribution function rather than assuming erroneously that the distribution is Maxwellian in radiation calculations.[9]

C. Description of Plasma

1. Classification of Plasma

The plasma conditions to be investigated include temperatures ranging from 5000°K to 8000°K (the boiling point of uranium is 4407°K at one atmosphere); a pressure of one atmosphere, and neutron fluxes ranging from 10^{12} to 10^{16} neutrons/(cm^2-sec). In determining the rate of occurrence of fission reactions, the uranium is assumed to consist entirely of the U^{235} isotope. Furthermore, the neutrons are assumed to be in thermal equilibrium with the plasma so that the fission cross-section

calculated by Bussard[33] is applicable, i.e., the effects of neutron spectrum hardening are negligible. In his calculation, the fission cross section weighted by the neutron flux distribution is averaged over energy, thereby eliminating the energy dependence of the cross section in favor of a characteristic temperature.

Upon fissioning, a uranium atom is assumed to split into two fission-fragments. The lighter fragment (96 amu) is born at 98 MeV and a charge of +16e, while the other is born at 67 MeV and a charge of +15e. The distribution of each fission-fragment is taken to be inversely proportional to energy.[10] The tendency of a fission-fragment to neutralize its positive charge as it thermalizes is included by assuming the fission-fragment's charge to be proportional to velocity.

In terms of the previously described energy extraction schemes, the plasma conditions cited above are characteristic of a subcritical uranium plasma. Also, this temperature range encompasses the 6000°K temperature of a proposed 5-MW experimental reactor.[11] The conditions of a critical plasma are somewhat hotter (center line temperature of 40,000°K[12]) and of higher pressure (approaching 500 atmospheres). However, the results for the plasma conditions to be studied should be applicable to the outer boundary layer of a critical plasma.

For the plasma parameters cited, the densities of the various plasma constituents can be predicted by the Saha equations[13] provided the necessary partition functions are known. Due to the lack of experimental data, the ratio of the partition functions is assumed to be unity (after Krascella[12]). The results for the Saha predicted densities appear in Fig. 1. A first order approximation of the perturbation to these densities

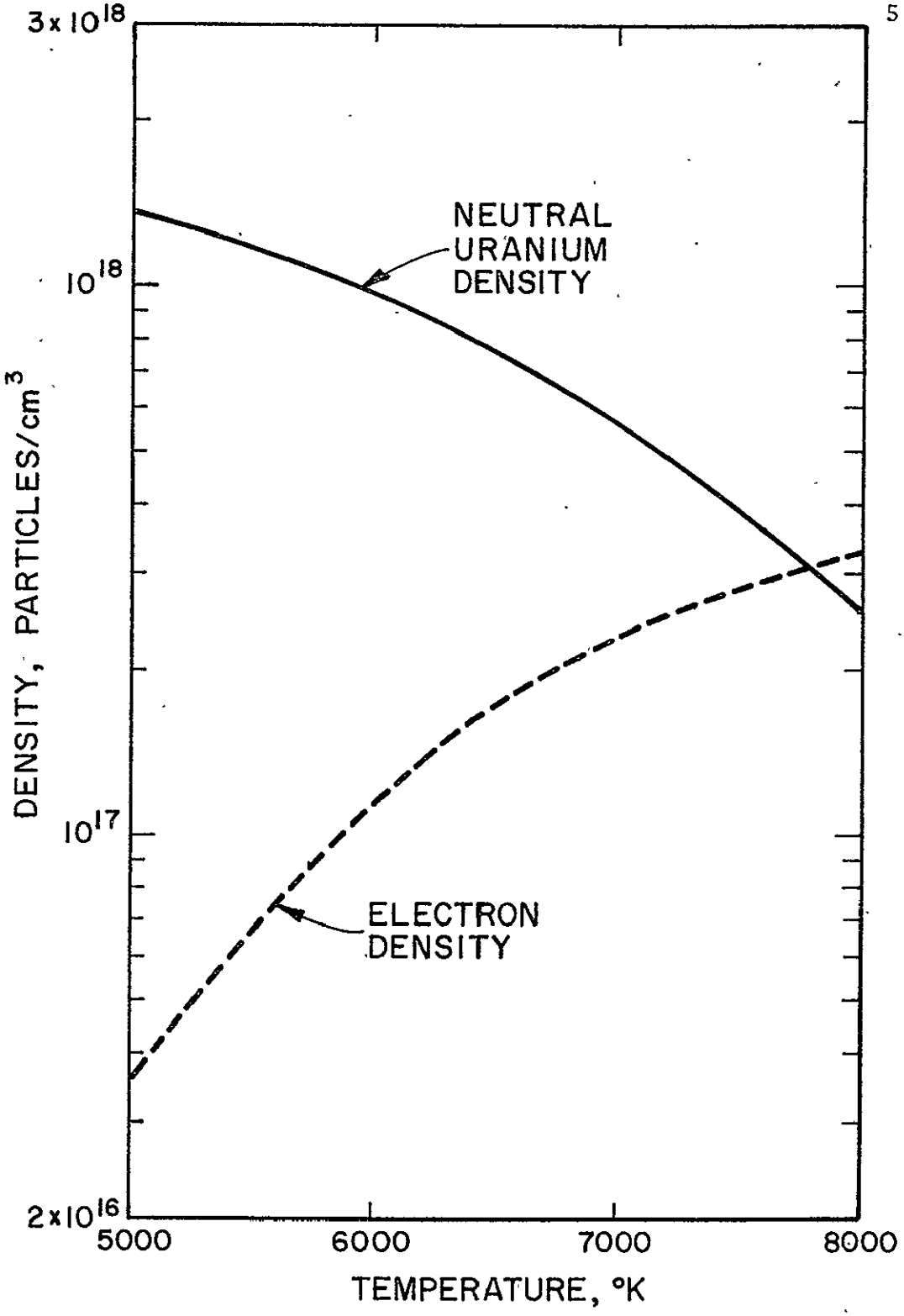

Fig. 1. The density of the uranium plasma constituents plotted versus temperature assuming a pressure of one atmosphere.

caused by the production of fission-fragment generated electrons is only of the order of 1/10% for cases of interest here. Therefore, a further correction for radiation effects is generally negligible.

With the electron densities and temperatures incurred, the plasma defies classification in classical terms (see Fig. 2). There exists an insufficient number of charged particles within a Debye sphere to provide the necessary screening of a charged test-particle required for the satisfaction of the binary collision assumption of the classical kinetic plasma. Similarly, the Landau distance of correlation is not sufficiently large for the plasma to be characterized by the very strong correlations of the classical collective plasma. Due to these difficulties, both a binary collisional treatment[14] and a unified treatment[15] which incorporates collective interactions as well as the binary collisions (see Appendix A) are applied to the Coulombic collisions.

2. Delineation of Collisional Processes

The dominant types of electron collisions present in the uranium plasma are: the aforementioned elastic Coulombic collisions--electron-electron and electron-ion scattering; and the inelastic collisions--ionization and excitation of neutral and singly ionized uranium (see Appendix B).

Since the inelastic cross sections have not been measured experimentally, they must be calculated from formulae based upon the Gryzinski model,[16] implementing the ionization and excitation data of Parks, et al.[17]

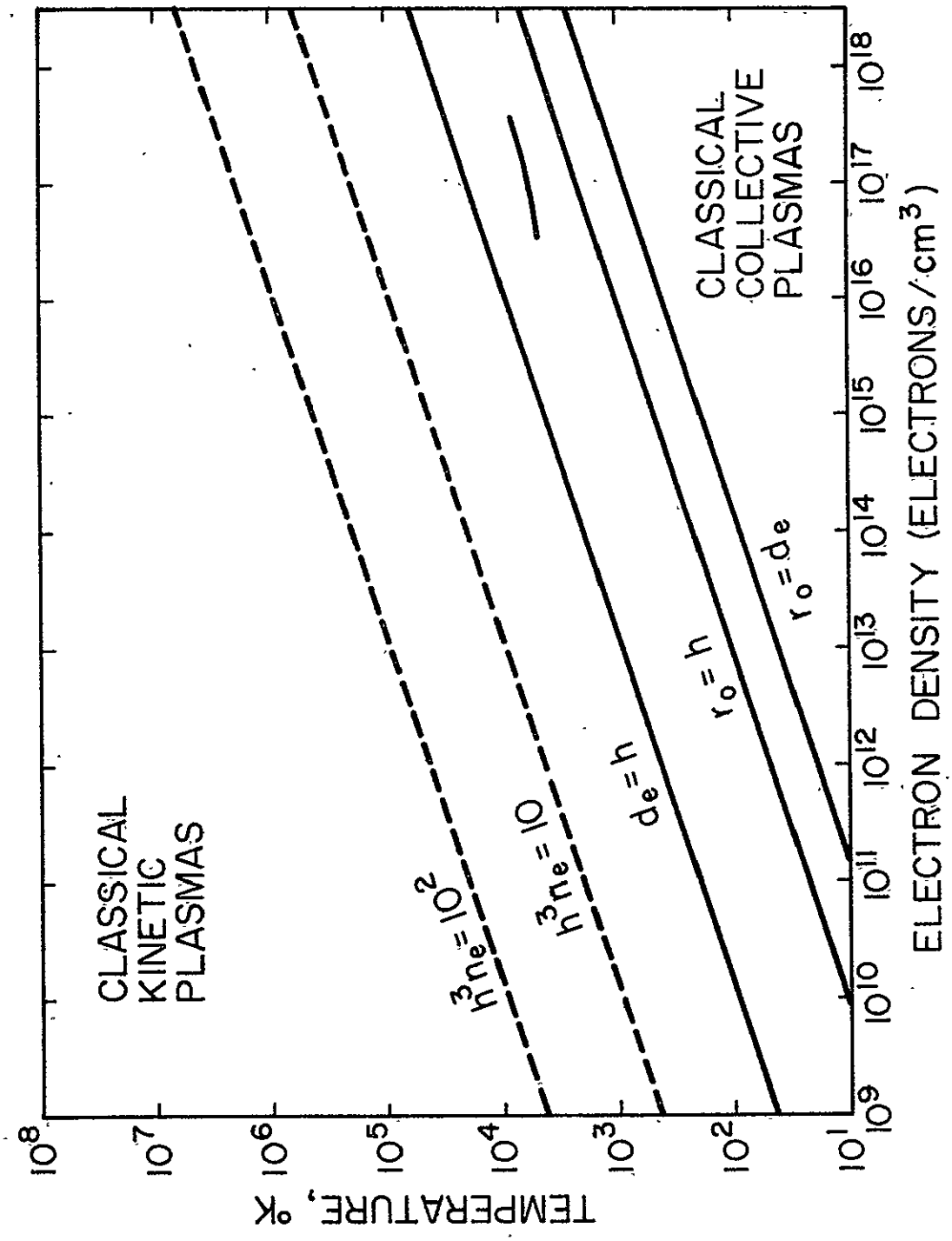

Fig. 2. A delineation of the plasma parameters defining the classical kinetic plasma and the classical collective plasma. The Debye length is given by h, the electron density by n_e, the charged particle spacing by d_e and the Landau correlation distance by r_o.

D. Methods of Solution

1. Governing Equation

The establishment of a governing equation for the distribution function is complicated by the presence of both inelastic and Coulombic collision types. For plasmas dominated by just one of these types, there exists a plasma equation describing the collision mechanisms involved. The Boltzmann equation, based upon the assumption that the duration of a collision is much less than the time between collisions, depicts binary collisions, short range forces, and neutral scattering; whereas the Fokker-Planck equation with a cut-off distance depicts Coulombic collisions which are not strictly binary in nature due to the long-range force responsible for the Coulombic interaction.[18]*

Then, the governing equation must be a combination of these two equation types in order to accommodate the presence of both collision types. Such an equation has been formulated by Dreicer[19] for a partially ionized gas. However, he included electron-neutral collisions which are negligible in the present case.

The distribution functions derived from both of these equations either separately or combined are one particle distributions. Such distributions fail to describe the correlation effects anticipated in a uranium plasma. They can only be described accurately by a many-bodied distribution which satisfies the Liouville equation. The complexity of this latter equation renders it impractical for direct use. However,

---

*Upon employment of the Coulombic cross section, the Boltzmann equation reduces to a Fokker-Planck type equation which is equivalent to the Fokker-Planck equation under special circumstances (see Montgomery and Tidman[20]).

the correlation effects can be approximately described within a specified error tolerance via the BBGKY hierarchy.[21] The Boltzmann and Fokker-Planck equations represent a zero order kinetic equation in this hierarchy while the first order equation is the Lenard-Balescu equation. The accuracy of these equations is expressed in terms of the assumed small plasma parameter $g = \frac{1}{n_e \lambda_D} << 1$, where n_e is the charged particle density and λ_D is the Debye length. The zero order kinetic equations are accurate to order 1, the first order kinetic equation is accurate to order g, the second order equation is accurate to order g^2, etc. In the uranium plasma, the assumption of g being small is not well satisfied. This presents a problem since the accuracy of even higher order equations becomes uncertain. Consequently, two sets of governing equations will be separately imposed: they are a combination Boltzmann and Fokker-Planck equation and a combination Boltzmann and Lenard-Balescu equation. It is argued that a comparison of the results will provide an estimate of the error introduced by not employing a many-bodied distribution function.

The previous equations may be simplified by noting the uranium plasma to be in a steady state. The presence of the high-energy electrons produced both by fission-fragments and other high-energy electrons creates a non-equilibrium state. However, the results of Lo[22] and Wang[23] at similar electron source rates indicate the source electrons relax into a Maxwellian distribution, with the non-equilibrium effects restricted to high energies. Then, the problem becomes one of investigating the relaxation of the high-energy tail into a Maxwellian distribution as described by the collision terms of the aforementioned equations.

2. Review of Methods and Proposed Solution

Most methods appearing in the literature are applicable to one equation type. Most notable of the methods are those of Rosenbluth, et al.[24] for the Fokker-Planck equation and those of Nighen[25] and Holstein[26] for the Boltzmann equation. They all expand the distribution function in terms of Legendre polynomials. Such methods are ideally suited to anisotropic plasmas with E-fields or injected beams.

In the present case, the assumption of an isotropic source and a primary interest in the high-energy tail make the method of Fano[27,28] much more appealing. However, provisions must be made to include a nascent or fission-fragment generated source distributed in energy plus a secondary electron source. The tractability of the resulting solution for the distribution function renders it an important tool for survey calculations and in the analysis of the distribution function.

In order to partially relax the assumption of continuous slowing down inherent in Fano's method, a Monte Carlo simulation is also performed which separates the Coulombic collisions from the inelastic collisions in a manner analogous to that of Wells[29] in earlier analytic studies. Unlike the Monte Carlo calculation of Thomas and Thomas,[30] the variation of the mean free path length with energy between the point of origin and the collision point is included in the calculation of the distance of random walk. Due to the presence of a secondary electron source, the ergodic hypothesis is not applicable so that a number of particles correlated in time must be considered simultaneously rather than repeatedly simulating an individual electron. The increased degree of sophistication of this calculation is obtained at the expense of the

economy of the solution. Then, the practical application of this technique would require that it be used solely as a check upon the validity of the analytic solution.

CHAPTER II

ANALYTIC SOLUTION

A. Introduction

In this chapter, a simple analytic formulation is sought for the relaxation of superthermal electrons into a thermalized ensemble of electrons which can be described by a Maxwellian distribution. The approach employed follows that of Spencer and Fano[28] for energetic electrons in an infinite medium, which predicts a distribution proportional to the inverse of the stopping power. Then, the resulting distribution will be a superposition of a high-energy tail on a Maxwellian thermal distribution. From this formulation, the effect of varying several plasma parameters can readily be predicted, or conversely, variations in the distribution can easily be traced to their source. The ease of analysis afforded by this method renders it an important tool for surveys, but the more detailed calculation of Chapter III must be retained if high accuracy is desired.

B. Derivation*

An analytic solution for the electron energy distribution function in an infinite medium can be derived from the following, completely general, expression for the conservation of electrons in energy space:

$$S(E)dE + g_{in} = g_{out} + \nu_c(E)f(E)dE \quad (1)$$

The distribution function f(E) represents the number of electrons per unit spatial volume per unit energy. The density of the electrons in the high-

*The derivation given here is a modification of one by Safanov.[31]

energy tail can be obtained as follows:

$$\int_{E_T}^{\infty} f(E)\, dE = n_{e_{E>E_T}} \tag{2}$$

where E_T is the threshold for non-Maxwellian behavior of the distribution function. The source function S(E) is equal to the electron production rate from all sources per unit spatial volume per unit energy. The rate at which electrons recombine is represented by $\nu_c(E)$. The rate of scattering from and into the energy interval dE about E is represented by q_{out} and q_{in}, respectively. For the energies of interest, the electrons which are scattered into the energy interval dE about E originate at energies greater than E; that is, the upscattering of electrons can be assumed to be negligible. Then, the electron balance expressed in Eq. (1) can be visualized as in Fig. 3.

The scattering terms appearing in Eq. (1) may now be evaluated. An expression for q_{out} may be obtained by dividing f(E)dE, the number of electrons in the energy interval dE about E, by a characteristic deceleration time τ_E, i.e.,

$$q_{out} = q_{out}(E) = f(E)\, \frac{dE}{\tau_E} \tag{3}$$

With the assumption of an infinitesimal energy loss per electron collision, dE/τ_E may be replaced by the rate at which electrons collisionally lose energy $\frac{dE}{dt}$. This is equivalent to the assumption of continuous slowing down. An additional implication of this assumption is that electrons scattered from one infinitesimal energy element dE about E + dE must be scattered into the adjacent element dE about E, i.e.,

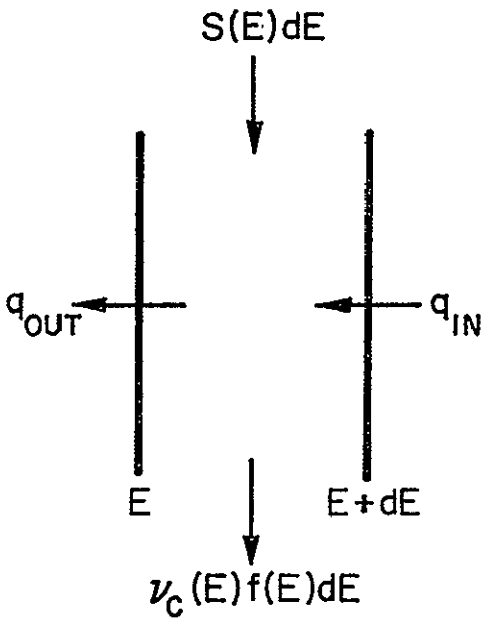

Fig. 3. The particle balance of Eq. (1) imposed upon the energy interval dE about E.

$$q_{in} = q_{out}(E + dE) \tag{4}$$

where q_{in} denotes the number of electrons/cm^3 slowing into the energy interval dE centered about E. Substitution of Eqs. (3) and (4) into the balance of Eq. (1) gives:

$$S(E)dE + f(E+dE)\left.\frac{dE}{dt}\right|_{E+dE} = f(E)\left.\frac{dE}{dt}\right|_{E} + \nu_c(E)f(E)dE \tag{5}$$

or

$$S(E) - \nu_c(E)f(E) = -\left\{f(E+dE)\left.\frac{dE}{dt}\right|_{E+dE} - f(E)\left.\frac{dE}{dt}\right|_{E}\right\}/dE \tag{6}$$

Invoking the fundamental theorem of calculus, Eq. (6) becomes

$$S(E) - \nu_c(E)f(E) = -\frac{d}{dE}\left\{f(E)\cdot\left.\frac{dE}{dt}\right|_{E}\right\} \tag{7}$$

Integration of Eq. (7) yields

$$\int_E^\infty \left\{S(E') - \nu_c(E')f(E')\right\}dE' = -\left\{f(E')\left.\frac{dE}{dt}\right|_{E'}\right\}\Bigg|_E^\infty \tag{8}$$

In the limit as E approaches infinity, the distribution function f(E) vanishes. Consequently, the distribution function must obey the following Fredholm integral equation

$$f(E) = \int_E^\infty \left\{S(E') - \nu_c(E')f(E')\right\}dE' \Big/ \left.\frac{dE}{dt}\right|_{E} \tag{9}$$

At high energies (at or above the inelastic collision threshold), recombination can be neglected. Defining the "cut-off energy" E_T such that recombination and upscattering are negligible for $E > E_T$, we obtain

$$f(E) = \frac{\int_E^\infty S(E')\,dE'}{\left.\frac{dE}{dt}\right|_E} \qquad , E > E_T \tag{10}$$

Strictly speaking, Eq. (10) is valid only for the steady state of an infinite, isotropic medium where continuous slowing down is applicable and external forces or fields are absent. The assumption of continuous slowing down has proved to be a valid assumption for elastic scattering off of heavy targets where the ratio of the energy lost to the original energy is small, as is evidenced by the successful application of the Fermi age theory[44] to the slowing of neutrons by heavy moderators. This assumption should also be valid for the Coulombic collisions where small angle scattering (hence, small energy transfer) is dominant. In the present case, however, inelastic scattering, i.e., ionization and excitation collisions, represents an equally important energy loss mechanism which does not necessarily comply with the continuous slowing assumption. This introduces some error into the model, thus, it can only be viewed as a first approximation. A more rigorous but more costly Monte Carlo treatment is then developed in Chapter III for more precise studies.

C. Numerical Solution

1. $\frac{dE}{dt}$

Numerical results for the distribution function can readily be obtained if $\frac{dE}{dt}$ and S(E) are known. Provided the collisions are of a binary nature, $\frac{dE}{dt}$ can be decomposed into a sum of energy loss rates for each type of collision, i.e.,

$$\frac{dE}{dt} = \left.\frac{dE}{dt}\right|_{\substack{\text{Coulombic}\\\text{collisions}}} + \left.\frac{dE}{dt}\right|_{\substack{\text{ionization}\\\text{collision}}} + \left.\frac{dE}{dt}\right|_{\substack{\text{excitation}\\\text{collision}}} \tag{11}$$

Both ionization and excitation collisions qualify as binary collisions. However, Coulombic collisions are not truly binary, yet they have been treated successfully as binary collisions in both applications of the Fokker-Planck equation[19] and in derivations of Fokker-Planck type equations.[14,20] Then, the decomposition of the energy loss rate in Eq. (11) is applicable to the present case.

Numerous treatments for $\left.\frac{dE}{dt}\right|_{\substack{\text{Coulombic}\\ \text{collisions}}}$ exist in the literature, such as the Fokker-Planck model.[14] The energy loss rates for ionization and excitation may be obtained by

$$\left.\frac{dE}{dt}\right|_E = \langle E \rangle_{loss} \cdot \sum v \qquad (12)$$

where v is the speed of a test electron relative to thermal electrons [v corresponds to the energy E in Eq. (10)] and Σ is the macroscopic inelastic cross section. The average energy loss per collision $\langle E \rangle_{loss}$ is defined as

$$\langle E \rangle_{loss} \equiv \frac{\int_0^\infty \frac{d\sigma(E,E')}{dE'} \cdot E' \, dE'}{\int_0^\infty \frac{d\sigma(E,E')}{dE'} \, dE'} = \frac{\int_0^\infty \frac{d\sigma(E,E')}{dE'} \cdot E' \, dE'}{\sigma(E)} \qquad (13)$$

where E is the energy of a test particle and E' is the energy lost by the test particle as a result of a collision. The microscopic cross section $\sigma(E)$ and the energy transfer differential cross section $\frac{d\sigma(E,E')}{dE'}$ for excitation and ionization events necessary for evaluating Eq. (13) have not been heretofore measured experimentally nor calculated. Then, these quantities had to calculated specifically for this study from a Gryzinski model[16] using the data of Parks, et al.[17] for uranium atom states (see Appendix B).

2. Iterative Solution of Source Term

The source term S(E) must include both secondary electrons and the nascent electrons resulting from ionization of uranium by fission-fragments. (Thermal electrons up-scattered in energy are excluded as they are negligible for most of the energy interval of interest.) Since the distribution of secondary electrons is dependent upon the distribution of nascent electrons and the manner in which they thermalize, a total source term S(E) cannot be known a priori. Consequently, S(E) and the distribution function f(E) must be calculated in an iterative manner as is described below.

First, the production rate of nascent electrons designated by $S_0(E)$ is calculated (See Section D). These electrons relax into a primary electron distribution $f_0(E)$ according to Eq. (10). During the thermalization process, the primary electrons further ionize the background uranium generating a source of secondary electrons $S_1(E)$. These secondaries distribute themselves in energy as prescribed by Eq. (10), i.e., insertion of $S_1(E)$ in the equation yields $f_1(E)$, producing yet another generation of secondary electrons $S_2(E)$. This process is continued until the sum of the $S_i(E)$'s converge to S(E) and likewise, the sum of the $f_i(E)$'s converge to f(E). The convergence of the sum of the $f_i(E)$'s is readily obtainable within a few iterations, in agreement with earlier observations of such a process by Fano and Spencer.[32]

D. Sample Results

1. Nascent Source

The starting point in the iterative scheme to determine the distribution function is the calculation of the nascent electron source S_0.

Since the electrons comprising S_o are the result of fission-fragment induced ionization of uranium, it is essential that the fission-fragment distribution is known. A simple estimate of this distribution can also be had from Eq. (10). The source of fission-fragments is so narrow in energy, it can be considered a delta function, i.e., two distinct fission-fragments are born, as the result of a single fission event, at energies of 67 MeV and 98 MeV and masses of 140 amu and 96 amu, respectively. Then, Eq. (10) becomes

$$f_{FF}(E) = \frac{S'}{\frac{dE}{dt}} \tag{14}$$

where S' represents the number of fission events/(cm^3-sec). Assuming a neutron flux of 2×10^{14} neutrons/(cm^2-sec), an averaged fission cross section of 57.6 barns,[33] and a gaseous uranium density of $5.6 \times 10^{17} cm^{-3}$ at 8000°K, S' is evaluated to be 6.5×10^9 fission-fragments of each kind are born/(cm^3-sec) in this example.

The fission-fragments experience electron capture over their entire track, i.e., $q = q_o V/V_o$ where q_o and V_o represent the initial charge ($\sim$16e) and velocity, respectively. Consequently, the energy loss dE/dx is a maximum at the beginning of their track. A semi-empirical formula[10] for the energy loss of a fission-fragment at energy E is given by

$$\frac{dE}{dx} \doteq \frac{2E_o}{\lambda(E_o)} \left(\frac{E_o}{E}\right)^{-1/2} \tag{15}$$

where E_o is the energy at which the fission-fragment is born and λ is its range (see Eq. 3.50 of reference 10 for a semi-empirical expression for λ). Then, the fission-fragment distribution is

$$f_{FF}(E) = \frac{\lambda(E_o)\, S'}{2E}\left(\frac{M}{2E_o}\right)^{1/2} \qquad (16)$$

where M is the mass of the fission-fragment and the relationship $dE/dt = V\, dE/dx = \sqrt{2E/M} \cdot dE/dx$ is utilized. The nascent electron source appearing in Fig. 4 is then obtained by averaging the fission-fragment distribution over a Gryzinski energy transfer cross-section for ionization events, generalized for heavy, multi-charged ions.[16] The average energy of the nascent electrons is found to be ∿10 eV.

2. Distribution Function

The results of successive iterations upon the distribution function are also shown in Fig. 4. Convergence is easily realized in three iterations. The final solution of the high-energy tail (dot-dash line) is displayed along with a Maxwellian distribution (solid line) corresponding to the plasma density and temperature previously cited. Where the high-energy tail intersects the Maxwellian, the source of electrons is no longer dominated by the nascent electrons and their resulting avalanche but rather by up-scattered electrons. Therefore, it is assumed in Fig. 4 that the actual distribution will more likely resemble a summation of the Maxwellian and the high energy tail.

3. Energy Loss Rate

The energy loss rates necessary for the calculation of the distribution function via Eq. (10) are displayed in Table 1. It is evident from the individual energy loss rates that the Coulombic collisions are as important in slowing down as are the inelastic collisions, ionization and excitation, inspite of the vast difference in the average energy lost per collision. Although the energy loss per collision by Coulombic interactions

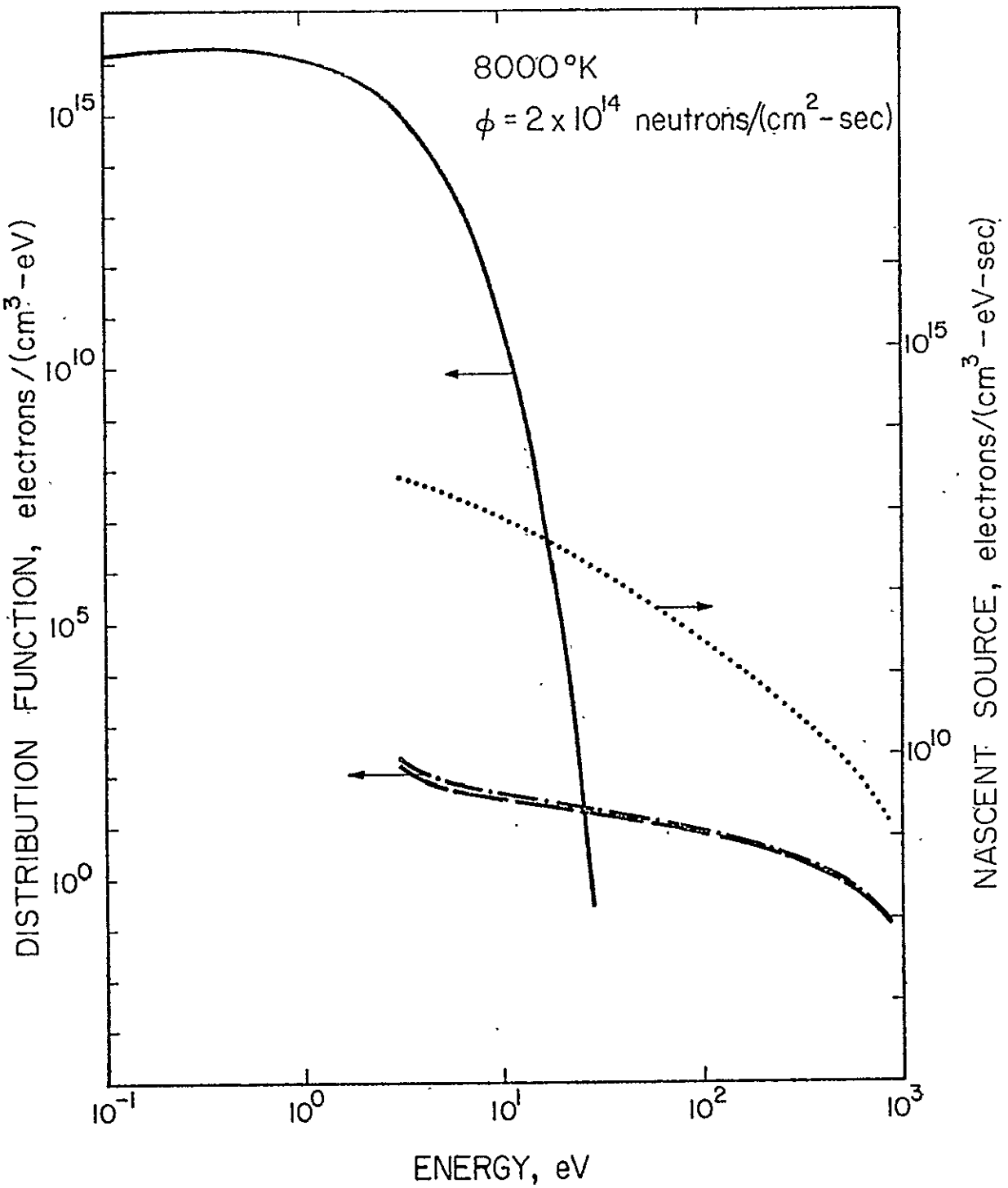

Fig. 4. The nascent source (....) versus energy as well as the distribution function plotted versus energy. The distribution consists of a Maxwellian (-) and the converged solution of the high-energy tail (-.-). The initial term in the series representation of f(E) is also plotted (--).

is small, the cross section is relatively large so that the loss rate for these events is comparable to inelastic loss rates.

For high energies, the largest permissable energy loss per collision is a half of an electron's energy before a collision. The probability of such a hard collision, either Coulombic or ionization, is small. Therefore, the assumption of continuous slowing is reasonable. However, at lower energies the energy lost in an ionization event can be a sizable fraction of the electrons original energy, and the continuous slowing approximation becomes less accurate.

For example, a crude estimation of the average energy loss per collision yields values of 25.9 eV and 2.9 eV for ionization and excitation collisions respectively for an electron at 32 eV, giving a $\Delta E/E$ of approximately unity, far too large for continuous slowing. In contrast, a similar estimation can be made for Coulombic collisions employing the expression for the electron collision frequency,[18]

$$\langle \nu_{ee} \rangle \simeq \frac{4}{3}(2\pi)^{1/2} n_e \left(\frac{e^2}{kT}\right)^2 \left(\frac{kT}{M_e}\right)^{1/2} \ln \Lambda \qquad (17)$$

where $\left(\frac{kT}{M_e}\right)^{1/2}$ is replaced by the velocity of an electron at 32 eV and the Coulomb logarithm is approximately 2.8. This yields a collision frequency of $\sim 4.5 \times 10^{13} \text{sec}^{-1}$, or ~ 0.044 eV lost/collision. Then $\Delta E/E$ is ~ 0.001 which is quite consistent with the continuous slowing assumption. Thus, as seen from Table 1, the results are expected to be more accurate for high temperatures where Coulombic collisions contribute a large fraction of the energy loss rate.

TEMPERATURE (1 Atm.)	ENERGY LOSS RATE, ergs/sec						TEST PARTICLE ENERGY, eV
	TOTAL	COULOMBIC COLLISIONS	U^o		U^+		
			IONIZATION COLLISIONS	EXCITATION COLLISIONS	IONIZATION COLLISIONS	EXCITATION COLLISIONS	
5000°K	2.26	.14	.60	1.45	.01	.06	826.2
	4.23	.24	1.13	2.70	.03	.13	179.3
	5.53	.36	1.28	3.68	.03	.18	57.0
	5.86	.45	1.14	4.04	.02	.21	26.0
	.60	.60	-	-	-	-	3.0
6000°K	2.13	.41	.43	1.03	.05	.21	826.2
	3.94	.72	.80	1.92	.10	.40	179.3
	5.24	1.04	.91	2.62	.09	.58	57.0
	5.71	1.29	.81	2.87	.06	.68	26.6
	1.40	1.40	-	-	-	-	3.0
7000°K	2.17	.81	.25	.60	.09	.42	826.2
	4.00	1.40	.47	1.12	.19	.82	179.3
	5.42	2.00	.53	1.53	.19	1.17	57.0
	6.11	2.45	.47	1.68	.13	1.38	26.6
	2.17	2.17	-	-	-	-	3.0
8000°K	2.23	1.13	.11	.27	.13	.59	826.2
	4.06	1.93	.21	.50	.27	1.15	179.3
	5.57	2.75	.24	.68	.26	1.64	57.0
	6.42	3.34	.21	.75	.18	1.94	26.6
	2.52	2.52	-	-	-	-	3.0

Table 1. Energy loss rates listed as a function of energy for various temperatures.

E. Parametric Results

1. Temperature Variation

The results of calculating the distribution function according to the analytic prescription of Eq. (10) for various temperatures are plotted in Fig. 5. The most noticeable effect of temperature variation is the increased magnitude of the deviation of the high-energy tail from the Maxwellian with decreasing temperature. This effect is directly traceable to the energy dependence of the average fission cross section[33] employed. As the plasma temperature and the corresponding average energy of the thermalized neutrons is decreased, the fission cross section increases, ultimately, yielding a larger nascent electron source rate (see Fig. 6). The degree of deviation from a Maxwellian as well as the energy range for which the non-Maxwellian behavior is dominant is thereby enhanced with decreasing temperatures. The point of intersection of the high-energy tail with the Maxwellian distribution denotes the lowest energy for which Eq. (10) is valid.

The effect of temperature variation upon the slopes of the high-energy tail is extremely subdued over most of its energy range. Only at the lowest energies, i.e., at the intersection of the high-energy tail with the Maxwellian, is there any noticeable difference. Examination of the energy loss rates in Table 1 reveals a partial explanation for the behavior of the slopes. The energy loss rates for the range of temperatures considered are more disparate at low energies. The inelastic cross sections fall off drastically at low energies, accounting for the low energy behavior of the energy loss rate while the temperature dependence of the density results in the energy loss rate being nearly independent

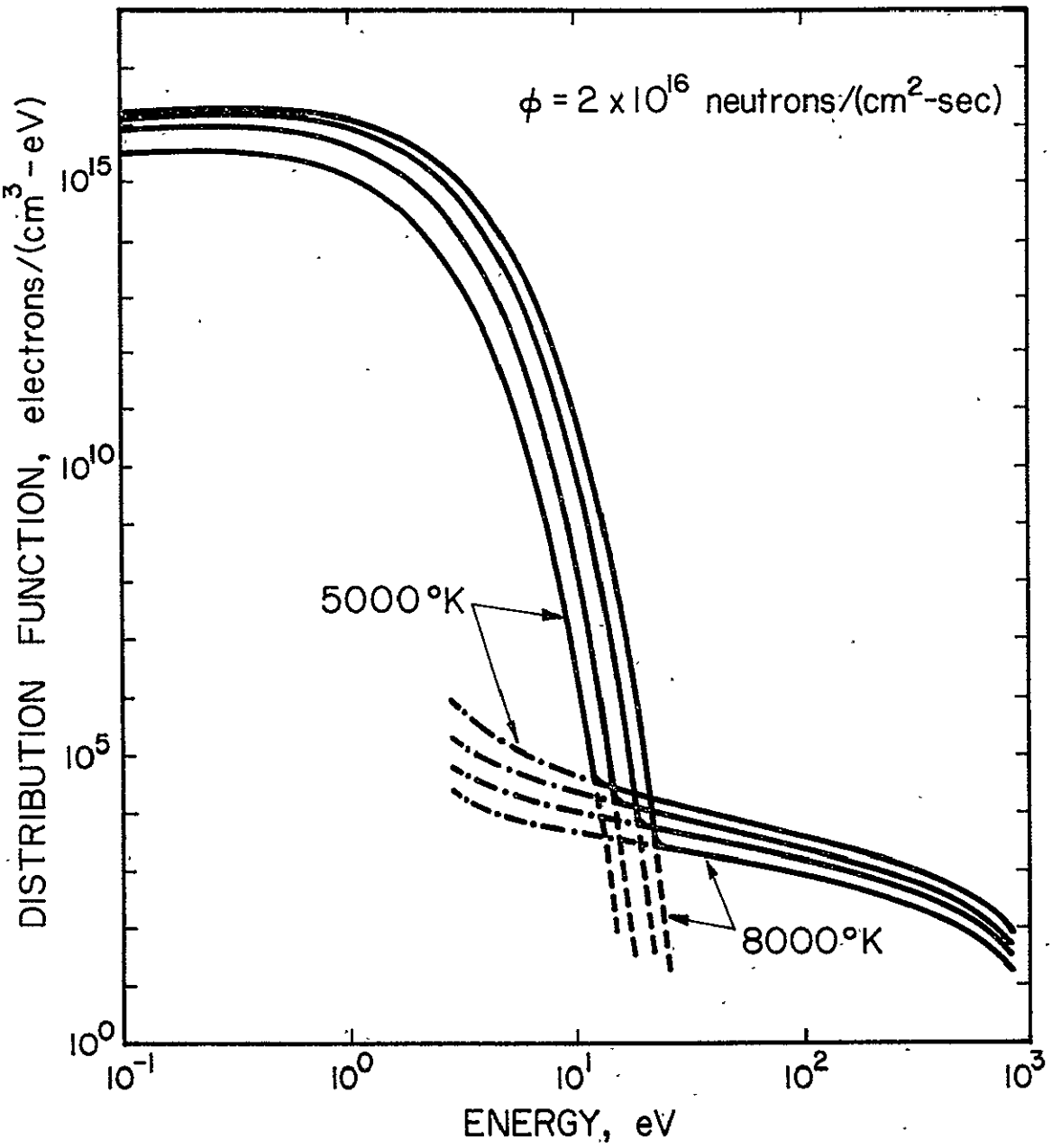

Fig. 5. The distribution function versus energy at a constant neutron flux of 2 x 10^{16} neutrons/cm^2-sec for temperatures of 8000°K, 7000°K, 6000°K, and 5000°K.

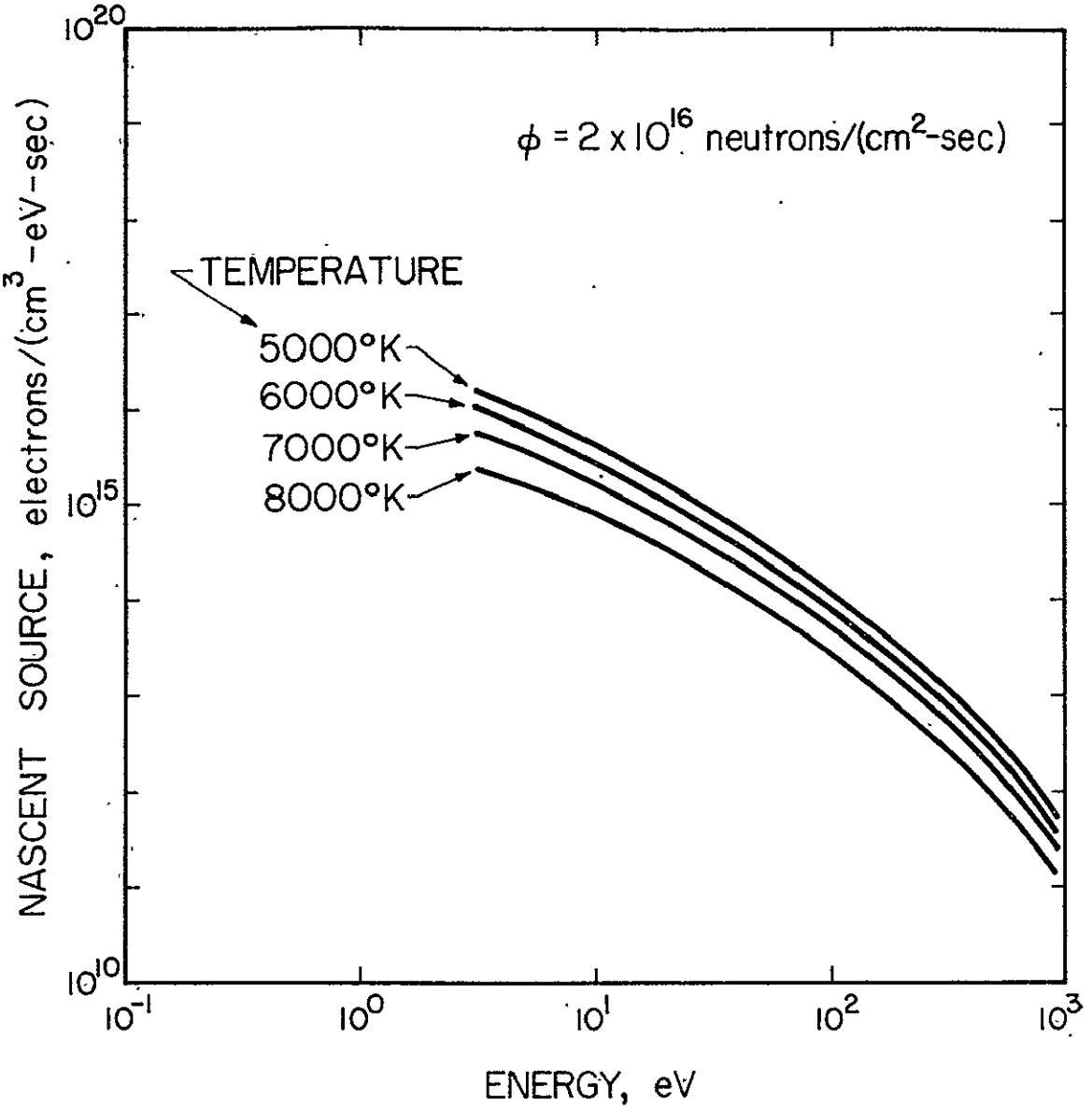

Fig. 6. The nascent sources employed in the calculation of the distributions of Fig. 5 versus energy.

of temperature at high energies.

A second factor influencing the slopes is the secondary electron source. Not only are the magnitudes of the sources different for the various temperatures considered but the shapes of the source distributions are different at low energies. The latter is caused by variations in the fraction of neutrals present in the plasma compound by difference in electronic structure between neutral uranium and singly ionized uranium. (This effect is observed only at energies near the threshold for ionization.)

2. Flux Variation

The effect of neutron flux variation upon the distribution function is considerably less complex than the effect of temperature variation. Under the plasma conditions studied, the bulk of the thermalized electrons is the result of the high plasma temperature. The neutron flux does not alter the thermalized densities by more than 1/10% from the normal Saha values. Then, the only effect a change in the neutron flux level can produce is a change in the production rate of high energy electrons. Therefore, according to Eq. (10), the high-energy tail is directly proportional to the neutron flux level, which is consistent with the results in Fig. 7 where the high-energy tail calculated at one flux level is simply a scaled vertical translation of the tail at a different flux level.

3. Cross-Sectional Dependence

A vital aspect of the interpretation of data is its credibility. The largest inaccuracy existing in the calculation of the distribution function lies with the uncertainty in cross-sections. Since no experimental data

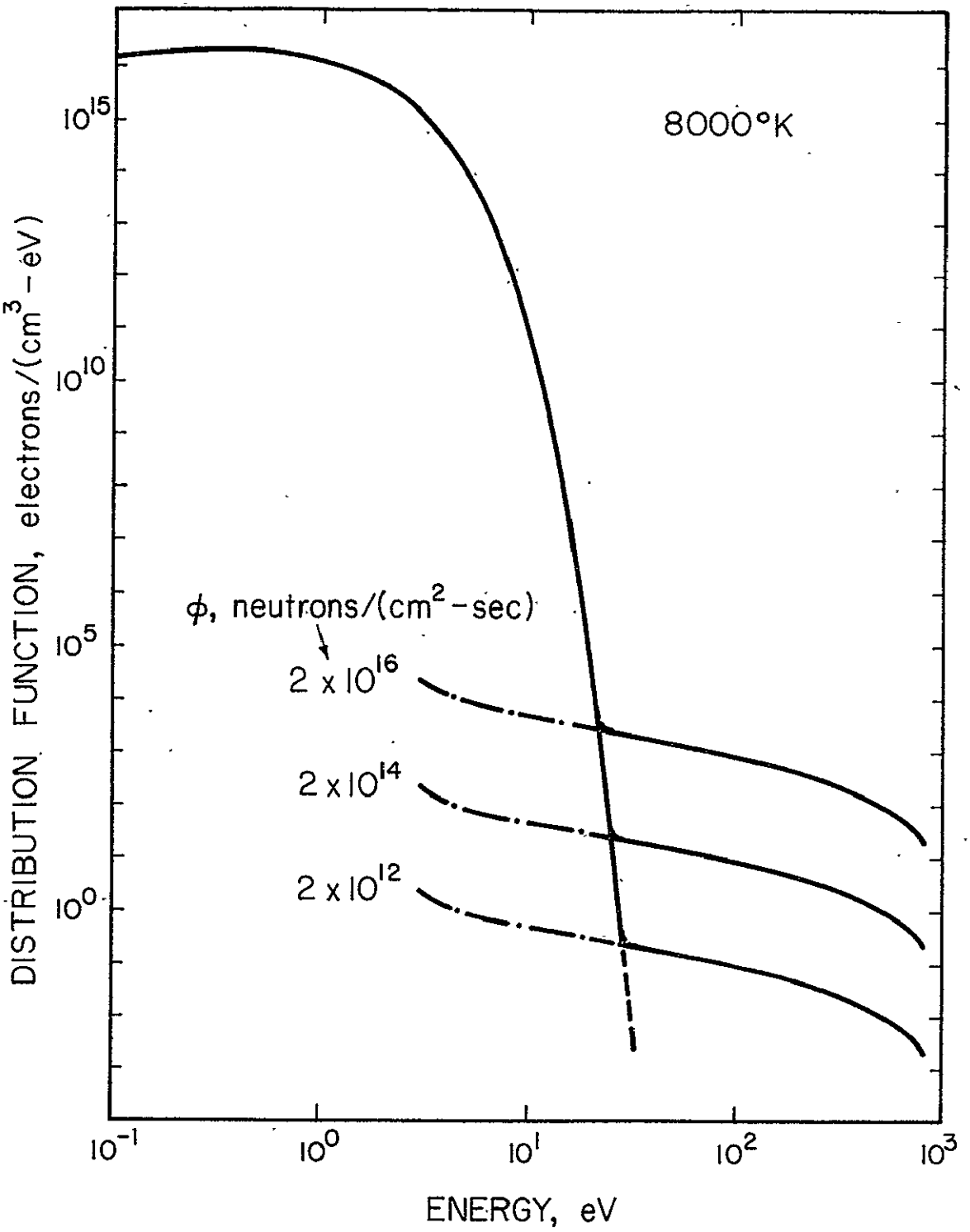

Fig. 7. The effect of varying the neutron flux upon the distribution function for a constant temperature of 8000°K.

exists for uranium, a hydrogenic model formed the basis for calculating the necessary cross-sections (see Appendix B). A comparison of the cross sections to measured values for cesium and helium reveals the uranium cross sections to fall between them, but closer to helium. However, due to the similarity in electronic structure of cesium and uranium, the uranium cross sections would be expected to lie closer to cesium than helium. To investigate this, another set of cross sections are obtained by doubling the inelastic cross sections. If the doubled cross-section set is used in the calculation of the distribution function in conjunction with the Coulombic energy loss rate predicted by the unified theory[15] (see Appendix A), the possible errors generated by inaccurate slowing theory can be gauged.

The result of just such a calculation is compared with a calculation with the unadjusted cross-section set and the Fokker-Planck slowing theory in Fig. 8. Fortunately, the differences indicated are not large, e.g., a maximum deviation of 4% is observed at $\sim$20 eV for 5000°K. Insight as to the reason for the differences can be gained from the energy loss rates appearing in Table 2 which were employed in this calculation and those in Table 1 for the previous calculations. Due to the doubling of the inelastic cross sections, both the source and the inelastic energy loss rates are doubled. Since $f(E) \propto S/\frac{dE}{dt}$, the factor of two is cancelled, provided the inelastic events dominate, as they do at 5000°K. At 8000°K, however, the increase in the source rate, a result of the ionization cross section being doubled, is not totally compensated by an increase in the inelastic energy losses. This occurs because of the relatively large contribution by elastic collisions at higher temperatures.

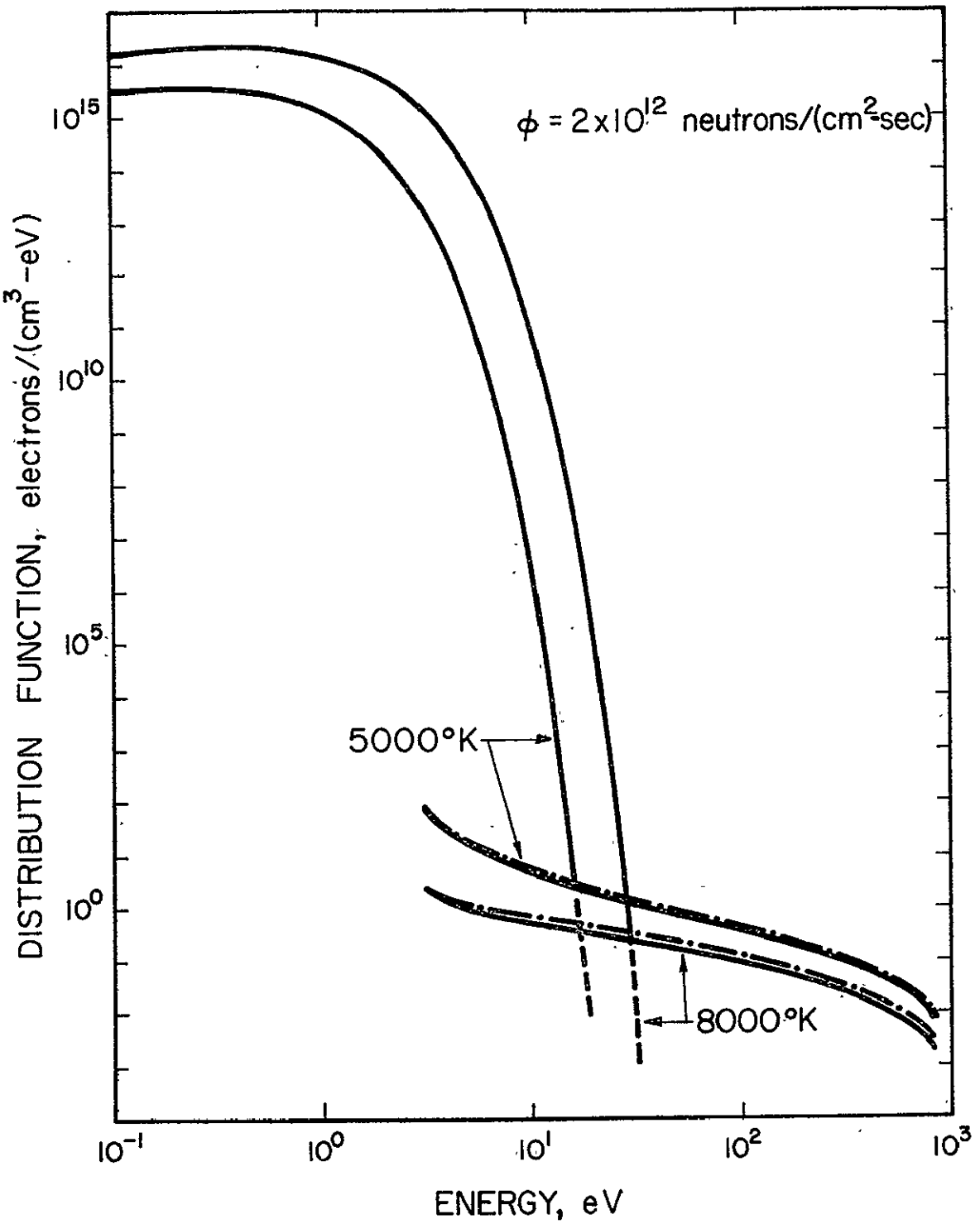

Fig. 8. The distribution function (-) versus energy compared to repeated calculation of the distribution with the cross-section set doubled (-•-).

TEMPERATURE	ENERGY LOSS RATE, ergs/sec						TEST PARTICLE ENERGY, eV
	TOTAL	COULOMBIC COLLISIONS	U^{o}		U^{+}		
			IONIZATION COLLISIONS	EXCITATION COLLISIONS	IONIZATION COLLISIONS	EXCITATION COLLISIONS	
5000°K	4.40	.14	1.20	2.90	.02	.13	826.2
	8.21	.24	2.26	5.40	.06	.25	179.3
	10.69	.36	2.55	7.36	.06	.36	57.0
	11.29	.47	2.28	8.07	.04	.42	26.6
	.87	.87	-	-	-	-	3.0
8000°K	3.33	1.13	.22	.54	.26	1.18	826.2
	6.24	1.97	.42	1.00	.55	2.31	179.3
	8.54	2.88	.47	1.37	.53	3.29	57.0
	9.80	3.64	.42	1.50	.37	3.88	26.6
	5.75	5.75	-	-	-	-	3.0

Table 2. Energy loss rates listed as a function of energy for various temperatures with the inelastic cross sections doubled and a unified theory treatment of the Coulombic collisions.

The errors projected in this section are indicative of those anticipated to appear in the calculation of the distribution function. The inelastic cross sections display a shape characteristic of other elements, most notably cesium, but are low in magnitude over all energies of interest by an estimated factor of two. The unified theory expression for the Coulombic energy loss rate more accurately depicts collective and binary interactions than the corresponding Fokker-Planck expressions, yet the difference is not so large as to discredit the Fokker-Planck result. From these results, it is seen that the anticipated inaccuracies in the inelastic cross sections and the Coulombic energy loss rate are compensating inaccuracies, i.e., the inaccuracy of the distribution is less than the inaccuracies associated with either the inelastic cross-section set or the Coulombic energy loss rate.

CHAPTER III

MONTE CARLO TECHNIQUE

A. Introduction

In the last chapter, it was pointed out that the assumption of continuous slowing is questionable, particularly at low energies. To treat the problem in a more precise manner, an improved treatment of inelastic collisions is required. Due to the increased complexity of the present treatment of the slowing process compared to the continuous slowing treatment, a Monte Carlo simulation was selected and is described here. A straightforward approach is to follow the electrons via an analytic prescription for Coulombic collisions for a time equal to the inverse of the inelastic collision frequency. At that time they suffer a discrete inelastic event which is treated by normal Monte Carlo techniques and then the process is repeated. The present method is an improvement over this technique in that provisions are made for the variation of the inelastic cross section between such events. Of course, the energy at which the inelastic collisions occur as well as the energy loss suffered are chosen in a random fashion according to the appropriate probability distribution.

B. Derivation of Governing Equation

The results of the previous section indicate the need to relax the assumption of continuous slowing down for inelastic collisions. An appropriate equation may be derived from Eq. (1), namely:

$$S(E)\,dE + q_{in} = q_{out} \tag{18}$$

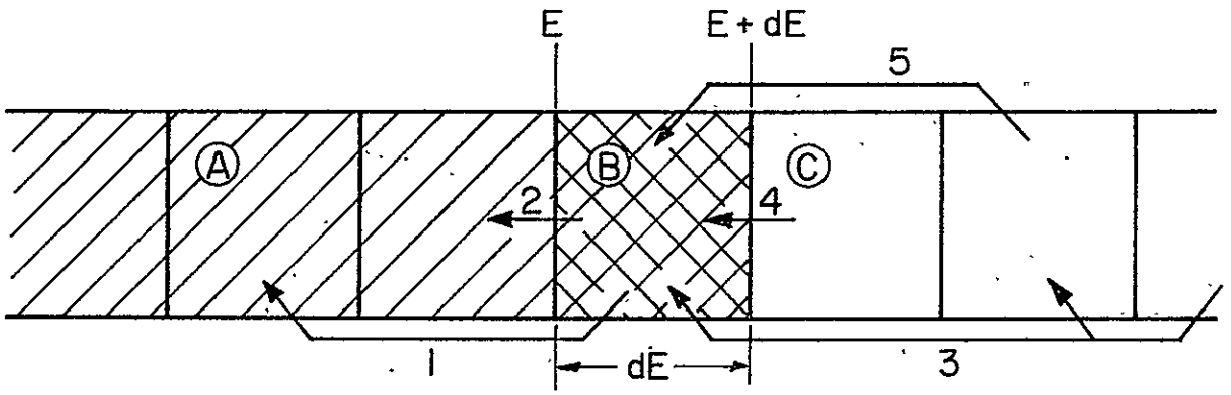

Fig. 9. Illustration of collisional processes used in the development of particle balance in energy space. The processes are: 1) inelastic scattering out of the interval dE about E 2) elastic (Coulombic) scattering out of the interval 3) secondary electron production in interval 4) elastic scattering into interval 5) inelastic scattering into interval.

where, as before, recombination is neglected. The slowing terms in energy space are readily obtainable from the diagram in Fig. 9.

The slowing down processes labeled 2 and 4 appearing in Fig. 9 are characteristic of the continuous slowing down model previously employed, but here it will be restricted to the elastic scattering component. Hence,

$$S(E)\,dE + f(E+dE)\left.\frac{dE}{dt}\right|_{E+dE} + q'_{in} = q'_{out} + f(E)\left.\frac{dE}{dt}\right|_{E} \tag{19}$$

where the primed terms indicate inelastic scattering. Expressions for q'_{in} and q'_{out} may be obtained with the Gryzinski[16] type energy transfer differential cross section $\frac{d\sigma}{d\varepsilon}(E,\varepsilon)$ introduced in Eq. (13). The term q'_{out} of Eq. (19) represents scattering via an inelastic process (represented by arrow 1 in Fig. 9) from the energy interval dE about E (the shaded region (B) in Fig. 9) into any energy interval dE below energy E (region A in Fig. 9). Mathematically, this can be written as,

$$q'_{out_1} = n\sqrt{\frac{2E}{m_e}}\left\{\int_0^{E_{max}} \frac{d\sigma(E,\varepsilon)}{d\varepsilon} f(E)\,d\varepsilon\right\} dE \tag{20}$$

where ε is the energy lost per inelastic scattering event, n is the density of the background species able to participate in the particular event under consideration, and the relative velocity is approximated by the velocity of an electron of energy E, i.e., $\sqrt{\frac{2E}{m_e}}$. The range imposed upon the energy lost ε varies from 0 to E_{max} which is determined by the process involved. Since there are a number of ionization and excitation processes competing in the slowing process, a sum over these processes is necessary, i.e.,

$$q'_{out} = \sum q'_{out_i} = \sum_i \left\{ n_i \sqrt{\frac{2E}{m_e}} \int_0^{E_{max_i}} \frac{d\sigma(E,\varepsilon)}{d\varepsilon_i} f(E)\, d\varepsilon \right\} dE \quad (21)$$

Similarly, the scattering process labeled 5 represents electrons of an energy greater than E (i.e., electrons from region C) which scatter into the energy interval dE about E, i.e.,

$$q'_{in} = \sum_i \left\{ n_i \int_0^{E_{max_i}} d\varepsilon \sqrt{\frac{2(E+\varepsilon)}{m_e}} \frac{d\sigma(E+\varepsilon,\varepsilon)}{d\varepsilon_i} f(E+\varepsilon) \right\} dE \quad (22)$$

Substitution of Eqs. (21) and (22) into Eq. (19) yields Eq. (23):

$$\begin{aligned} & S(E)\,dE + f(E+dE) \left.\frac{dE}{dt}\right|_{E+dE} \\ & \quad + \sum_i \left\{ n_i \int_0^{E_{max_i}} d\varepsilon \sqrt{\frac{2(E+\varepsilon)}{m_e}} \frac{d\sigma(E+\varepsilon,\varepsilon)}{d\varepsilon_i} f(E+\varepsilon) \right\} dE \\ & = \sum_i \left\{ n_i \sqrt{\frac{2E}{m_e}} \int_0^{E_{max_i}} d\varepsilon \frac{d\sigma(E,\varepsilon)}{d\varepsilon_i} f(E) \right\} dE \\ & \quad + f(E) \left.\frac{dE}{dt}\right|_E \end{aligned} \quad (23)$$

The source term S(E) appearing in Eq. (20) may be decomposed into a series as was done in Chapter II. The first term S_0 in the series represents the nascent electron source while additional higher order terms depict the various generations comprising the avalanche of secondary electrons. A concise expression for the total secondary electron source may be derived from considerations of the ionization process labeled 3 in Fig. 9. The secondary electrons born in the energy interval dE about E are the result of ionization collisions in which an incident electron

loses an energy $E + U_i$ where E is the secondary's kinetic energy and U_i is the energy necessary for the secondary electron to overcome the ionization potential of the target uranium atom. Due to the indistinguishability of electrons, the least energetic of the resulting pair is defined as the secondary electron and the other, more energetic electron is defined as that electron which was termed the incident electron before the collision occurred. Then, integration of the ionization reaction rate over the energy range of electrons capable of generating a secondary electron of energy E followed by a summation over the various bound electronic states which can participate in secondary electron production yields the following expression for the total electron source rate:

$$S(E)dE = S_o(E)dE + \sum_{i\geq 1} S_i(E)dE$$

$$= S_o(E)dE + \sum_i \left\{ n_i \int_{E+U_i}^{E_{max_i}} d\mathcal{E} \sqrt{\frac{2(\mathcal{E}+E+U_i)}{m_e}} \frac{d\sigma(\mathcal{E}+E+U_i, E+U_i)}{d\mathcal{E}_i} f(\mathcal{E}+E+U_i) \right\} dE \quad (24)$$

The calculation of the nascent source term S_o is outlined in Chapter II. Then,

$$S_o(E)dE + \sum_i \left\{ n_i \int_{E+U_i}^{E_{max_i}} d\mathcal{E} \sqrt{\frac{2(\mathcal{E}+E+U_i)}{m_e}} \frac{d\sigma(\mathcal{E}+E+U_i, E+U_i)}{d\mathcal{E}_i} f(\mathcal{E}+E+U_i) \right\} dE$$

$$+ f(E+dE)\left.\frac{dE}{dt}\right|_{E+dE} + \sum_i \left\{ n_i \int_0^{E_{max_i}} d\mathcal{E} \sqrt{\frac{2(E+\mathcal{E})}{m_e}} \frac{d\sigma(E+\mathcal{E}, \mathcal{E})}{d\mathcal{E}_i} f(E+\mathcal{E}) \right\} dE$$

$$= \sum_i \left\{ n_i \sqrt{\frac{2E}{m_e}} \int_0^{E_{max_i}} d\mathcal{E} \frac{d\sigma(E,\mathcal{E})}{d\mathcal{E}_i} f(E) \right\} dE + f(E)\left.\frac{dE}{dt}\right|_E \quad (25)$$

The governing equation can be obtained from Eq. (25) by invoking the fundamental theorem of calculus, i.e.,

$$S_o(E) + \frac{d}{dE}\left\{ f(E) \left.\frac{dE}{dt}\right|_E \right\}$$
$$+ \sum_i n_i \int_0^{E_{max_i}} d\varepsilon \sqrt{\frac{2(E+\varepsilon)}{m_e}} \frac{d\sigma(E+\varepsilon,\varepsilon)}{d\varepsilon_i} f(E+\varepsilon)\, d\varepsilon$$
$$+ \sum_i n_i \int_{(E+U_i)}^{E_{max_i}} d\varepsilon \sqrt{\frac{2(E+\varepsilon+U_i)}{m_e}} \frac{d\sigma(E+\varepsilon+U_i, E+U_i)}{d\varepsilon_i} f(E+\varepsilon+U_i)$$
$$= \sqrt{\frac{2E}{m_e}} \sum_i n_i \int_0^{E_{max_i}} d\varepsilon \frac{d\sigma(E+\varepsilon)}{d\varepsilon_i} f(E) \qquad (26)$$

The inelastic collision terms in Eq. (26) have been derived elsewhere.[22] However, their appearance with the continuous slowing down treatment is unique.

C. Simulation

1. Distinction Between Collisional Processes and Their Treatments

a. Coulombic Collisions

Equation (26) is not amenable to an analytic solution as was Eq. (7), but it does lend itself to a novel method of solution involving a Monte Carlo simulation that integrates both analytic and random walk techniques. An analytic description of the Coulombic collisions is employed in the tracing of the histories of electrons. An individual electron is permitted to evolve for a time Δt as prescribed by the following equation.

$$\int_t^{t+\Delta t} dt \left.\frac{dE}{dt}\right|_{\substack{\text{Coulombic}\\ \text{collision}}} = \Delta E \qquad (27)$$

where $\left.\frac{dE}{dt}\right|_{\substack{\text{Coulombic}\\ \text{collision}}}$ represents the electron energy loss rate due to Coulombic

collisions[14,15] and ΔE is the energy lost during the time Δt. Then, if an electron has an energy E associated with it at time t, at time $t + \Delta t$ its energy is $E - \Delta E$. The inelastic collisions are then superimposed on the Coulombic slowing down in a discrete fashion as described below.

b. Inelastic Collisions

i. Choice of Collision Energy

Since the inelastic collisions are less frequent than the Coulombic collisions, they are superimposed in a random walk fashion. The distance of the walk is prescribed by a probability distribution dependent upon the test particle's energy, the inelastic cross-sections, and the Coulombic energy loss rate. Such a function can be obtained by first examining the probability P(x) of a collision occurring in an infinitesimal distance dx about x measured along the flight path of an electron. This probability is a product of the macroscopic cross section Σ for inelastic collisions and the length of the interval dx, i.e., $\Sigma(x)\,dx$. The functional dependence upon x is included as a reminder that the inelastic cross section depends on energy which in turn is dependent upon the distance of travel within the slowing medium. The density of the target particles is assumed to be constant within the medium.

The probability of traveling a distance x without a collision is the ratio of the intensity of a beam of test particles displaced a distance x to the initial intensity at $x = 0$, i.e., $I(x)/I(0)$. The attenuation of such a beam is governed by the following equation:

$$-dI(x) = \Sigma(x)\, I(x)\, dx \tag{28}$$

Integration of Eq. (28) yields,

$$\frac{I(x)}{I(0)} = \exp\left(-\int_0^x \Sigma(x')\,dx'\right) \tag{29}$$

Then, the probability of the first inelastic collision occurring in dx about x is

$$P_1(x)\,dx = \left\{\exp\left(-\int_0^x \Sigma(x')\,dx'\right)\Sigma(x)\right\}dx \tag{30}$$

Since the problem is to be solved in energy space, an equivalent probability of the first inelastic collision occurring in the energy interval dE about E is desired, or

$$P_1(x)\,dx = P_1(E)\,dE \tag{31}$$

thereby implying that the Jacobian necessary for such a transformation would be $\frac{dE}{dx}$ which can be related to the energy loss rate by,

$$V\left.\frac{dE}{dx}\right|_E^{\text{Coulombic collisions}} = \left.\frac{dE}{dt}\right|_E^{\text{Coulombic collisions}} \tag{32}$$

Then, the transformation of Eq. (30) into the energy variable E yields Eq. (33):

$$P_1(E)\,dE = \left\{\exp\left(-\int_{E_0}^{E} dE'\,\Sigma(E')\,\frac{\sqrt{\frac{2E}{m_e}}}{\left.\frac{dE}{dt}\right|_{E'}^{\text{Coulombic collisions}}}\right\}\frac{\Sigma(E)\sqrt{\frac{2E}{m_e}}}{\left.\frac{dE}{dt}\right|_E^{\text{Coulombic collisions}}}\,dE \tag{33}$$

where $P_1(E)$ is the probability that the first inelastic collision will occur at energy E if the electron is injected at energy E_o.

ii. Determination of Energy Lost

Once it has been established that a collision occurs at energy E, the amount of energy lost must be determined. This too is prescribed by

a probability distribution function. The probability of a particle which collides at energy E losing energy ε may be obtained by normalizing the differential energy transfer cross section $\frac{d\sigma}{d\varepsilon}(E,\varepsilon)$ to the microscopic cross section $\sigma(E)$ for that process, i.e.,

$$P_T(\varepsilon)d\varepsilon = \frac{d\sigma(E,\varepsilon)}{d\varepsilon}\,\frac{d\varepsilon}{\sigma(E)} \tag{34}$$

The determination of the process, i.e., which of the uranium species, collision types, and atomic levels are involved, must preceed the energy loss calculation (see Appendix C for the algorithms employed).

2. Merging of Treatments

a. No Inelastic Collision

The manner in which all of the above aspects of collisions are incorporated to yield a complete description of the slowing down process will now be illustrated with an example. Let us begin by assuming an electron is born at energy E_o which corresponds to a time t_o on the energy vs. time plot on the right hand side of Fig. 10. This plot, generated according to Eq. (27), represents an electron's energy as a function of time as it slows down solely due to Coulombic collisions in an intermediate energy range well above E_T. Since the introduction of source particles must occur frequently enough to approximate continuous interjection, an individual electron is only permitted to evolve for some small time interval Δt. The result of one such period is to let the electron follow the slowing down curve to the point corresponding to time $t_1 = t_0 + \Delta t$ and energy E_1. A second period leaves the electron at time $t_2 = t_0 + 2\Delta t$ and energy E_2. This process continues until that period in which the electron falls below the energy E_T for which Eqs. (7) and (13) become in-

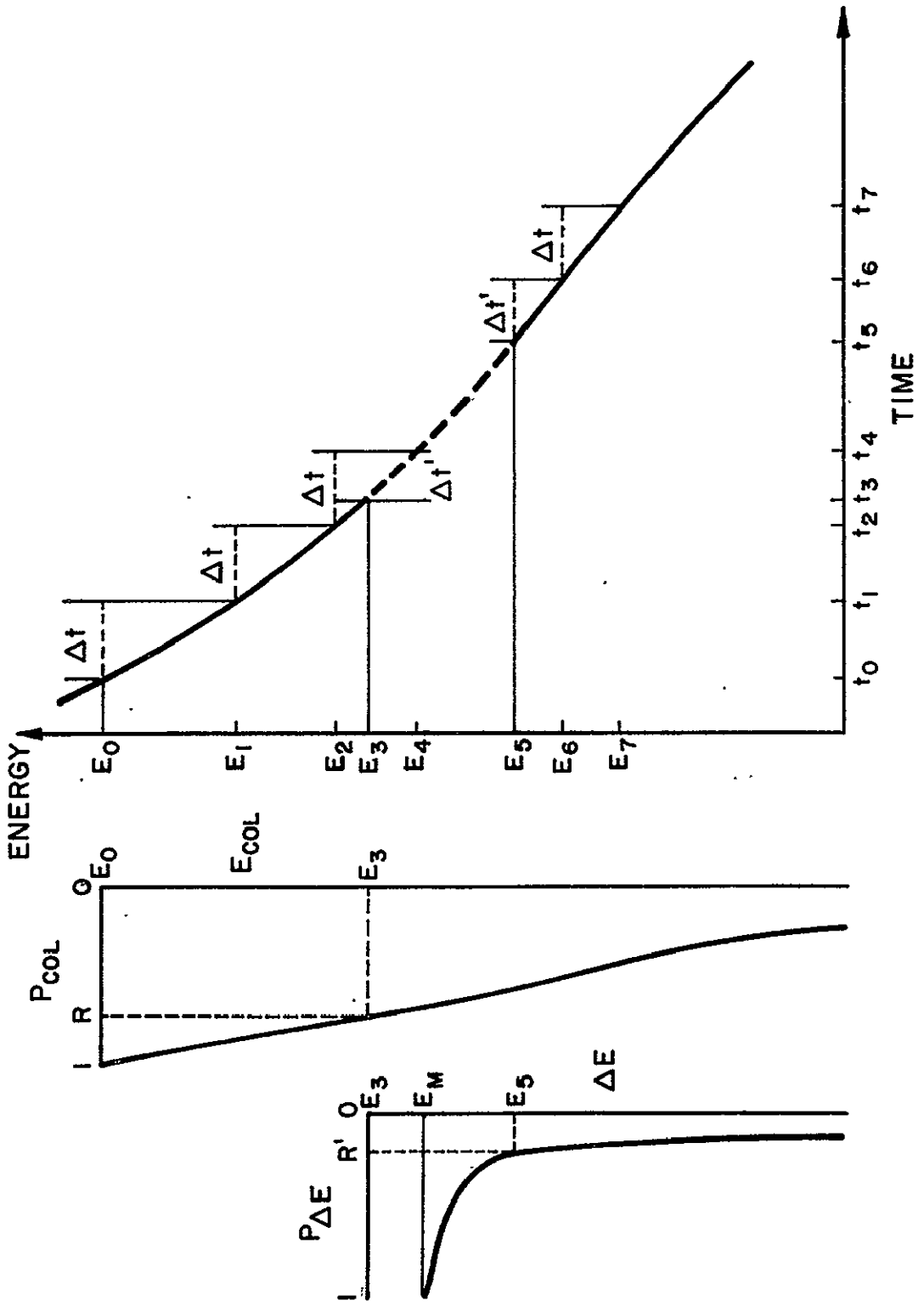

Fig. 10. Scheme for electron simulation. Figure contains plots of energy versus time as predicted by Eq. (27), of the collision probability P_{col} versus collision energy from Eq. (37) and of the probability of losing energy ΔE in an inelastic collision $P_{\Delta E}$ versus final electron energy from Eq. (38).

valid, or an inelastic collision occurs.

b. Inelastic Collision

The decision for the existence of an inelastic collision must be made at the beginning of the electron's history, i.e., at E_o. It is based upon the probability of an electron traversing the energy range E_o to the lowest valid energy considered E_T, or the non-collision probability:

$$P_{NC} = \exp\left(-\int_{E_o}^{E_T} dE' \Sigma(E') \frac{\sqrt{\frac{2E'}{m_e}}}{\left.\frac{dE}{dt}\right|_{E'}^{\text{Coulombic collisions}}}\right) \tag{35}$$

This probability is by necessity equal to one minus the integral of the probability of a collision occurring at energy E, Eq. (33), with the limits of integration being from E_o to E_T. Comparison of P_{NC} with a random number chosen from the range 0 to 1 completes the decision process. If the random number is greater than P_{NC}, then an inelastic collision must occur. Conversely, if the random number is less than P_{NC}, the electron will not suffer an inelastic collision.

For the sake of thoroughness, assume the electron collides. Then, the energy at which the collision will occur must be selected. Normally, the energy would be randomly selected from the inverse distribution of the probability of colliding at energy E. However, if the probability distribution is too complex to invert, as it is here, a form of the rejection technique[34] must be employed. This algorithm begins by mapping the probability distribution onto a rectangle of unit area. The prescription for obtaining an acceptable candidate for the collision energy E involves the selection of two random numbers, r_1 and r_2, where r_1 represents an evaluation of the probability distribution and the other, r_2, is a candidate for E. If r_1 is less than the distribution evaluated at r_2, then r_2

is accepted as the collision energy. However, if the converse is true, the candidate is rejected and the process is repeated until an acceptable candidate is found. (This process is analogous to throwing darts at a rectangle with the coordinates of the impact point corresponding to r_1 and r_2. When the impact point falls below the probability distribution, the corresponding energy is taken to be the collision energy.)

As applied to the calculation of the energy of the next collision, the technique commences with the following prescription for the renormalized collision probability:

$$P_{COL} = \frac{P_1(E_{COL})}{P_1(E_o)} \tag{36}$$

where the expression for P_1 is obtained from Eq. (33) and the energies E_{col} and E_o are, respectively, a candidate for collision energy and the initial electron energy. Inherent to the success of the algorithm is that the maximum value of the probability distribution is readily obtainable, i.e., the maximum must occur at E_o. Then,

$$P_{COL}(E_{COL}) = \left\{ \exp\left(-\int_{E_o}^{E_{COL}} dE' \frac{\sum(E')\sqrt{\frac{2E'}{m_e}}}{\left.\frac{dE}{dt}\right|_{E'}^{\text{Coulombic collisions}}} \right) \right\} \frac{\sum(E_{COL})\sqrt{\frac{E_{COL}}{E_o}} \left.\frac{dE}{dt}\right|_{E_o}^{\text{Coulombic collisions}}}{\sum(E_o) \left.\frac{dE}{dt}\right|_{E_{COL}}^{\text{Coulombic collisions}}} \tag{37}$$

A plot of P_{col} versus E_{col} also appears in Fig. 10.

The choice of collision energy is completed by first randomly choosing a candidate E_3 from the energy range E_o to E_T. Next the corresponding $P_{col} = R$ is calculated and compared with a random number in the interval 0 to 1. If the random number is less than R, the candidate energy E_3 is accepted as the site of the collision. If the random number is greater than R, the process is repeated until an acceptable candidate is obtained.

Continuing the present example, the collision energy is assumed to be E_3. Then the electron slows from energy E_0 to E_3 via Coulombic collisions. In the third time period, the period in which the collision occurs, the electron would have proceeded from time t_2 and energy E_2 to time $t_4 = t_2 + \Delta t$ and energy E_4 if a collision had not occurred. The occurrence of a collision does not alter the fact that the electron must interact via Coulombic collisions for the full time period Δt (the inelastic interaction time is negligible compared to Δt). Then, after the occurrence of the inelastic collision, Coulombic interactions are to be resumed for a time $\Delta t'$ in order to complete the evolution of the electron for the period Δt.

The determination of which of the background species is involved and also which of the possible ionization and excitation events will be involved in the collision must precede the calculation of the energy lost as a result of the collision. The species selection is accomplished by a comparison of a random number (henceforth in the discussion all random numbers are assumed to be evenly distributed from 0 to 1) to the ratio of the macroscopic cross section of a species to the total macroscopic cross section in the usual Monte Carlo fashion. Similarly, the type of collision is chosen by comparison of a random number with the ratio of the microscopic cross section for a species process to the total microscopic cross-section.

For economical reasons, the energy lost in an excitation collision is approximated as the excitation energy. This approximation is a reasonable one because the possible energy losses range from the excitation energy of the process considered to the excitation energy of the net

state affording a larger energy transfer. Furthermore, the difference in energy of two adjacent excitation levels is usually small compared to the excitation energy (see Table 4) and the probability of an energy transfer event increases as the amount of energy transferred decreases.

In the case of an ionization collision, the amount of energy lost by the electron at energy E_3 is also determined by a rejection technique. In this case, the renormalized probability $P_{\Delta E}$ is

$$P_{\Delta E} = \frac{P_T(\Delta E)}{P_T(E_M)} \tag{38}$$

where $P_T(\Delta E)$ is the probability of losing ΔE energy through an ionization collision and is obtained from Eq. (34). The energy E_M represents the minimum energy which can be lost and is non-zero because of the presence of a threshold energy necessary to initiate the ionization process.

In Fig. 10, a plot of $P_{\Delta E}$ is presented as a function of the final energy (rather than the energy transferred). As before, a candidate E_5 is chosen as the energy of the electron after the collision and the corresponding renormalized probability $P_\Delta(E_5)$ is subjected to the acceptability criterion. Assuming R' to be larger than the random number chosen, the tracing of the electron can proceed from energy E_5.

At this point a decision is made whether or not the electron will incur further collisions and where in energy the next collision will occur. This is done as previously described. After performing these tasks, an attempt is made to permit the electron to proceed a time $\Delta t'$ such that the period will be completed. The electron is advanced to energy E_6 corresponding to time $t_6 = t_5 + \Delta t'$, provided a collision does not occur at an energy greater than E_6. Should another collision occur in the same

period, the previous process is repeated until the electron has been permitted to evolve for the duration of the time period Δt, and so the evolution continues for additional periods, moving in steps of Δt along the Coulombic slowing down curve, to the next collision and eventually past the threshold energy of validity E_T.

3. Computational Time Reduction

Five additional techniques are utilized to provide a substantial reduction in computational time without altering the accuracy of the code. The techniques are described below in the order of their effectiveness.

The first technique is a unique, new method called convergence propagation. A necessary criterion for its applicability is that f(E) is dependent upon f(E' > E) (rather than f(E' < E)). Then, capitalizing upon this condition, the method is the dynamic expansion downward in energy of the energy region over which the distribution is simulated. The expansion of the simulation region occurs only when convergence has been obtained in the current region. The savings in computational time is realized by not having to simulate the distribution below energy E until the wave of convergence has arrived at E (for a more detailed discussion of this technique, see Appendix C).

A second technique involves the fitting of frequently evaluated, complex functions with a number of quadratic equations, each valid in a unique subinterval of the dependent variable's range. The coefficients of these equations are determined by a cubic spline algorithm (from the IMSL subroutine library). The savings are substantial, and better than single precision accuracy is easily obtained for the functions.

A third technique is strongly coupled to the convergence propagation technique in that an optimum time step is chosen for each energy group in the convergence scheme. The time for an electron to traverse the various energy groups varies by four orders of magnitude in the present problem. Thus, it becomes essential to gear the frequency at which convergence is checked, i.e., Δt, to the group transit time of the current converging group as the convergence wave propagates towards lower energies. Deviations in the specification of Δt as the transit time are permitted by examining the ratio of the number of electrons in the group to the number of source electrons introduced. If the source is the major input into the group, then Δt is shortened from the transit time. Conversely, if the source is not the dominant input, then a larger time is used to permit sufficient collisions to occur in order to get better statistics on the input into the group due to inelastic collisions. By this scheme, the convergence check will be made as soon as a significant change has been made in the distribution function.

A fourth technique relies upon stacking source particles in energy and staggering their associated time of introduction. At the time of particle introduction or replenishment, m particles, where $m = k \cdot \ell$ (m, k, ℓ are integers), are introduced into an energy interval, where ℓ particles are assigned the same injection energy, there being k such energies. To avoid the m particles behaving as if only k particles had been introduced, each is assigned a unique collision energy and associated time of injection. Since particles are replenished with a periodicity of Δt, an assigned injection time t must lie randomly within the interval $T_i - \Delta t < t < T_i$ is the time at which the current replenishment occurs

according to the internal clock. Many facets of the time consuming calculation of the collision energy are thereby retainable for the other ℓ-1 particles at the same energy.

A fifth technique involves the utilization of an initial guess. The proximity of the guess to the ultimate answer determines the efficiency of this technique. However, the effectiveness of this technique as reported by Wang[23] was not realized in the present Monte Carlo code. This is attributed to the effectiveness of the convergence propagation technique.

D. Test Run

Immediate questions arising after the development of a Monte Carlo code concern the accuracy and the rate of convergence to the solution of the proposed problem. The criterion for convergence involves various conditions such as: consistency, approximity to an experimentally observed quantity or independent calculation, and stability of the solution. Each of these tests are stringently applied to an arbitrarily chosen case in the ensuing paragraphs.

The case in question is for a neutron flux of 2×10^{16} neutrons/(cm^2-sec) and a plasma temperature of 5000°K. A sample of the results is shown in Fig. 11. The figure is a composite of four graphs, each depicting the high-energy tail at successive times as recorded by an internal clock. Also appearing in each graph is the tail of a Maxwellian distribution corresponding to the electron density and temperature, and the corresponding analytic solution for the high-energy tail. As in Chapter II, the total distribution function in either the Monte Carlo or analytic calculation is the union of the Maxwellian and the corresponding high-energy tail.

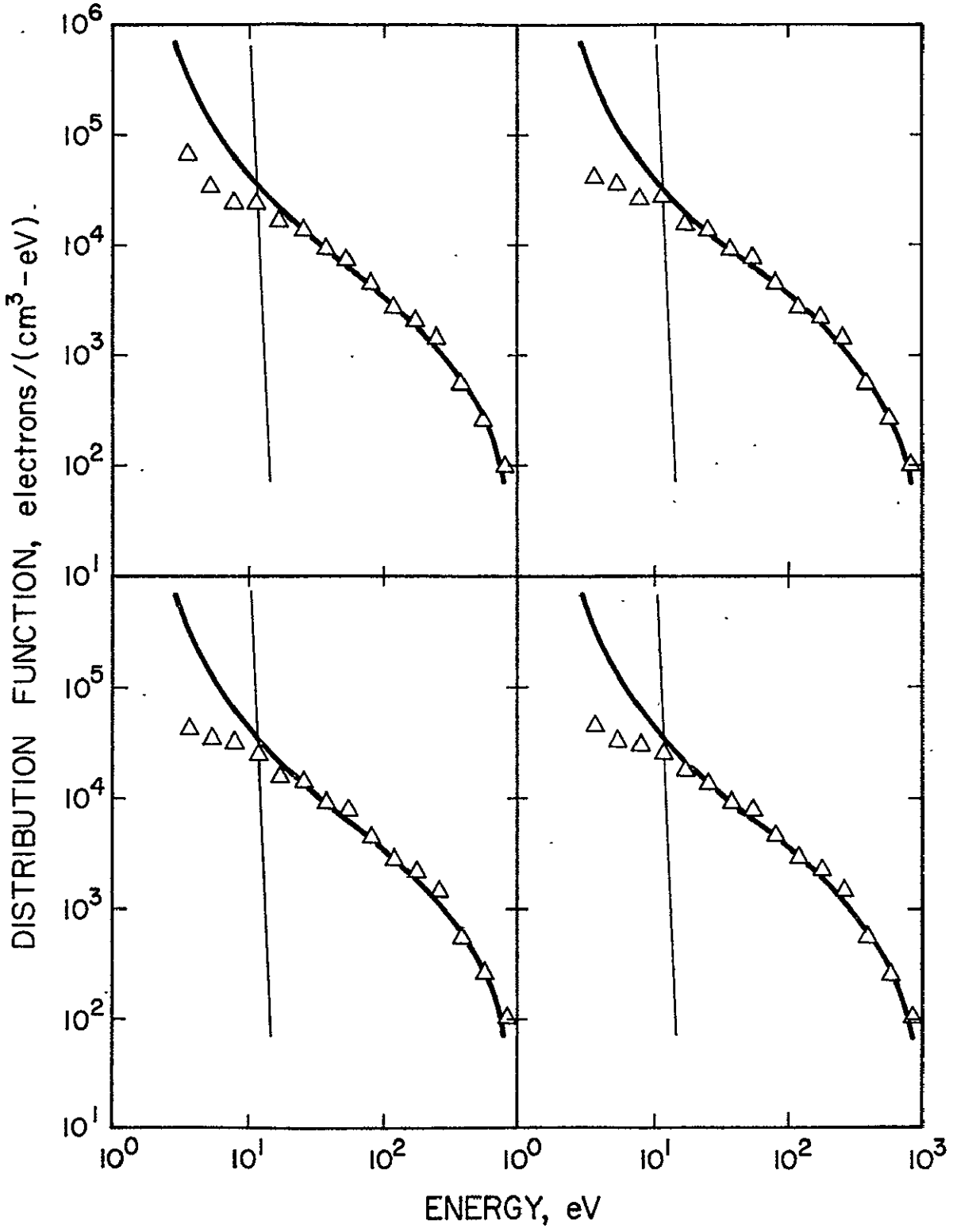

Fig. 11. Snapshots of Monte Carlo distribution (Δ's) at four different times. Also displayed are a Maxwellian distribution (light line) and the analytic solution (dark line).

The relationship between the analytic and Monte Carlo result is atypical of other temperatures and shall be explored in detail in Section F of this chapter. For the present, the analytic result will serve solely as a standard for comparison. The final result to be reported later is an average of a dozen such snapshots of the distribution function.

1. Consistency

Since a computed result may seem plausible and yet be erroneous, especially with large computer programs such as the present Monte Carlo code, the code must be established to be free of programming and logic errors. This is accomplished by comparing, for consistency, computer calculations with independent hand calculation.

The aforementioned computer results are not those of the distribution function, but rather additional, supplemental results relative to the distribution function, recorded at the time of each snapshot. A sample of these results, corresponding to the last snapshot of Fig. 11, appears in Fig. 12. Each entry in Fig. 12 is briefly described below.

The energy lost by all the electrons within an energy group centered at the tabulated energies is recorded, providing information regarding the slowing mechanisms. The presence of zeros in the ionization and excitation energy loss rate columns indicates there were no collisions of this type during the last time period Δt.

Also, the W-value (the energy lost per ion pair formed) is calculated during the same time period. This particular value is larger than the average value based upon results at eleven other time periods, i.e., 160 eV per ionization event. The importance of this particular result cannot be fully realized as there are no experimental measurements with

$\frac{DE}{Dt} \times 10^4$ ergs/(sec-cm^3)			ENERGY, eV	
COULOMBIC COLLISIONS	EXCITATION COLLISIONS	IONIZATION COLLISIONS		W-VALUE: 203.2 eV/(per ion pair formed)
2.9	0.6	0.0	823.7	
5.8	0.0	73.6	558.9	
9.6	0.0	0.0	379.2	THE ELAPSED TIME:
20.0	2.9	211.1	255.3	4.8 NANOSECONDS
23.8	2.0	0.0	174.6	
22.1	2.6	0.0	118.5	
29.7	0.0	55.0	80.3	
39.0	0.0	0.0	54.5	
33.4	2.9	0.0	37.0	
36.6	1.6	3.2	25.1	
37.0	5.2	1.8	17.0	
40.5	3.8	5.0	11.6	
37.0	1.6	0.0	7.8	
29.2	0.0	0.0	5.3	
16.2	0.1	0.0	3.6	

GROUP BALANCE

Number of Particles out (x 10^3 electrons/cm^3	≈	Number of Particles in (x 10^3 electrons/cm^3)				
Electrons scattered out	≈	Secondary Electrons	+	Nascent Electrons	+	Electrons Scattered In
267.2	≈	2.5	+	34.6	+	223.5

GLOBAL PARTICLE BALANCE

Number of Particles out (x 10^3 electrons/cm^3)	≈	Number of Particles in (x 10^3 electrons/cm^3)		
Electrons Scattered out	≈	Secondary Electrons	+	Nascent Electrons
267.2	≈	33.0	+	232.3

Figure 12 Additional Computer Results

which to compare and the result is plagued by a large statistical uncertainty. However, the result is consistent with the expectation that it be larger than the ionization potential of 6.2 eV for neutral uranium.

The time elapsed on the internal clock is presented in comparison with an estimate of the time necessary to achieve a converged solution by a straightforward Monte Carlo simulation. If the elapsed time is larger than the estimated time, then the electron slowing calculation is grossly in error even if the initial guess is very poor. Then, a value of 3.6 for the ratio of the estimated time to the elapsed time is reassuring concerning the validity of the electron slowing. This factor of 3.6 is also a measure of the efficiency of the convergence propagation technique.

The data necessary to determine if particle balances exist for the lowest energy group and the entire ensemble of energy groups appears in Fig. 12. A particle balance to within a tolerance of ±15% is imposed upon the current lowest group as a condition for advancing to the next group in the convergence propagation scheme. If the lowest energy group complies with this condition, then a snapshot of the high-energy tail is recorded. No provisions are made to guarantee a global particle balance. Then, the observance of such a balance to within ±1% insures the validity of the propagation of convergence technique and the accuracy of the integral of the distribution function.

Further consistency checks can be performed with the data in Fig. 12 For example, the total Coulombic energy loss rate at 25.1 eV divided by the number of particles within the group, f(E) dE (where it is correctly assumed that all the electrons in the group suffer this collision-type) yields an energy loss rate of .41 ergs/sec. The average value obtained

for a dozen snapshots is .45 ergs/sec. These values are within ten percent of the calculated value, in Table 1, of .448 ergs/sec.

For inelastic collisions, the energy loss rate is tabulated as the result of two separate algorithms; one establishes the collision frequency while the other determines the energy loss. A separate run specifically designed to check the average energy loss produced results very similar to those calculated in Section D of Chapter II. The mean value of the energy loss for excitation collisions, 2.98 eV, obtained from the code is comparable to an average value of 2.9 eV calculated in Chapter II. For ionization events, the code generated values of 23.4 eV compared to an average value of 24.5 eV also calculated in Chapter II.

The accuracy of the collision frequency algorithm can also be verified by comparing the number of excitation collisions generated by the code with the number of expected excitation collisions as calculated below. Dividing the excitation energy loss rate at 25.1 eV of Fig. 12 by an average energy loss of 2.98 eV yields a value of 3.43×10^{15} excitation collisions per second. Alternately, since there are 8.3×10^{5} electrons at 25.1 eV and the collision frequency is 8.7×10^{9} collisions/sec, 7.2×10^{15} excitation collisions are expected per second. These results are in reasonable agreement, and the discrepancy can be attributed to statistical fluctuations as the average excitation energy loss obtained from the Monte Carlo code is 3.2×10^{4} ergs/sec compared to the value of 1.63×10^{4} ergs/sec reported for this particular snapshot of the distribution function. From these checks, the code can be concluded to be a consistent and accurate representation of the physical processes involved.

2. Approximity to Independent Result

Confidence in the Monte Carlo calculations can also be gained by a comparison with the results of the earlier analytic model. The two results are in exceedingly good agreement in Fig. 11. However, such exceptional agreement is atypical (see Fig. 18). Nevertheless, the assumption of continuous slowing down, which is the basis of the analytic model, is not too unreasonable under the plasma conditions considered here. Therefore, the approximity of the two models' results is expected and its observance (see Fig. 18) reaffirms our confidence in the Monte Carlo calculations. Furthermore, the existence of a display of common trends (see Section E) and a predictable disparity (see Section F) reinforce the acceptability of the Monte Carlo solution.

3. Stability

The final criterion for the acceptability of the solution is its exhibition of stability. The stability of the "converged" solution is displayed in Fig. 11 over a short period of time while a longer term time history of the distribution evaluated at a single energy is shown in Fig. 13. In both instances, random oscillations about an average value are observed. The display of this type of behavior in conjunction with the observance of a global particle balance suggests that the solution has converged. However, these criteria for convergence are not acceptable until they have been demonstrated to correctly predict the solution to be stable for extended periods of time (at least several multiples of the Coulombic slowing down time).

The necessity of observing the distribution then for tens of nanoseconds imposes a severe financial strain. Thus, a less costly, but

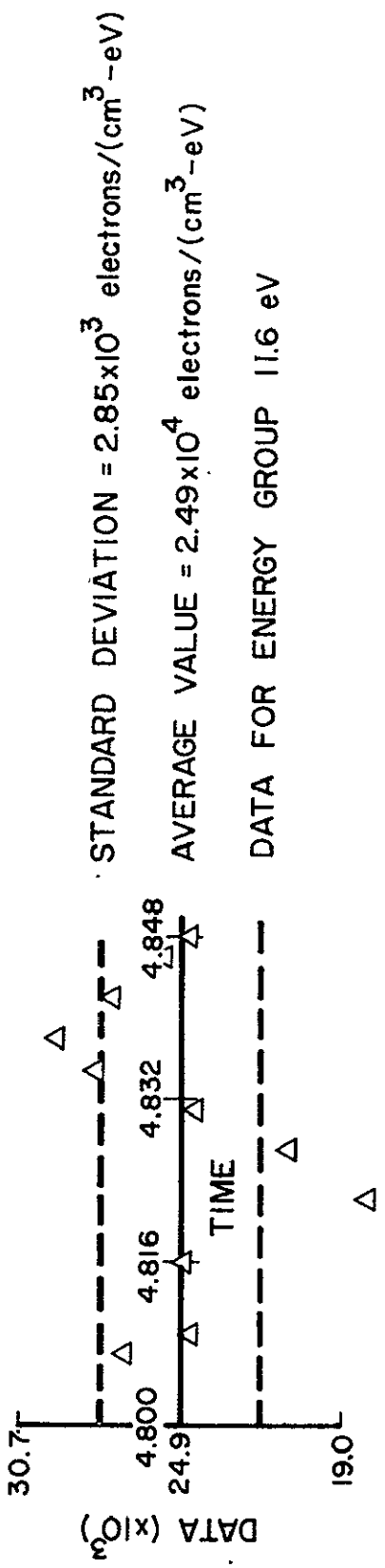

Fig. 13. The history in time of an individual point f(E) on the Monte Carlo curves of Fig. 11 (Δ's)

equivalent scheme of sustained observation, was ultimately employed. The scheme relies on the knowledge that a necessary condition for terminating observations is the elimination of any correlation in time of the last observation with the initial observation. In Monte Carlo calculations, this is equivalent to using a random number string of infinite period or several strings of large but finite period. Then, by repeating the calculation several times, each time using a different random number string, sufficient data will exist to determine if the solution has relaxed into a stable configuration.

Such tests were performed for a distribution at 8000°K. This particular temperature was chosen because the final distribution differs most from the initial guess, the analytic solution. The results of a dozen observations taken in six separate runs of the code, with different random number strings for each run, are summarized in Table 3. Each average of the dozen observations for the six runs falls within a standard deviation of the average of all seventy-two observations, except for the values at the two lowest energies. The reason for the bad statistics at low energies lies in the choice of the machine particle distribution (see Appendix C). Since these two distribution points are past the intersection of the Maxwellian and are not meaningful, their behavior is irrelevant. The observance of oscillations in the standard deviation are the result of the coarseness imposed upon the calculation through the number of simulation particles utilized, combined with the fact that an electron will, on the average, suffer three inelastic events while slowing from 1 keV to 3.0 eV for an 8000°K plasma.

These tests were repeated at 5000°K, but with only three separate runs (and three random number strings). As before, an average of the dozen observations recorded in a single run falls within a standard deviation of the average of all thirty-six observations. Furthermore, at 8000°K and 5000°K, the standard deviation calculated in each run approximately equals the standard deviation of all observations at the same temperature. Then, a single run yields sufficient data from which to conclusively generate the converged solution. The converged solution is the average of the dozen observations recorded in a single run to within a standard deviation, also calculated in the run (see Table 3 for typical values of the standard deviation).

E. Parametric Studies

1. Temperature Dependence

The resulting distribution functions of Monte Carlo calculations are displayed in Fig. 14 for various temperatures at a constant neutron flux of 2×10^{14} neutrons/(cm^2-sec). The overall trends indicated by the Monte Carlo results are quite similar to the earlier analytic solutions in Fig. 5. The distribution function appears to be dependent upon temperature variations predominantly through the normalization of the high energy tail, except for a slight change in slope at low energies.

2. Neutron Flux Dependence

Similarly, the distribution functions calculated by the Monte Carlo code reflect the same trends in parametric variations of the neutron flux as do the analytic results, namely, the distribution function is directly proportional to the neutron flux level. This is amply illustrated in Fig. 15 for a plasma temperature of 5000°K.

DISTRIBUTION FUNCTION, electrons/(cm^3-eV)				ENERGY, eV
AVERAGE VALUE	STANDARD DEVIATION, %	MAXIMUM VALUE	MINIMUM VALUE	
.10	6.3	.110	.089	823.7
.30	4.8	.329	.278	558.9
.56	12.5	.73	.455	379.2
.94	15.7	1.27	.73	255.3
1.47	8.5	1.69	1.24	174.6
2.23	5.6	2.54	1.91	118.5
3.07	12.0	3.98	2.54	80.4
3.81	6.1	4.50	3.34	54.5
4.57	8.2	5.43	3.95	37.0
6.05	7.6	7.09	5.01	25.1
7.56	7.3	9.85	5.85	17.0
8.39	10.5	11.23	5.50	11.6
9.24	12.0	14.01	6.74	7.8
10.42	19.2	17.14	7.34	5.3
12.06	32.4	24.99	7.72	3.6

Table 3. Statistical data on Monte Carlo results for 8000°K and a neutron flux of 2×10^{14} neutrons/(cm^2-sec) based on a dozen observations each of six runs with different random number strings.

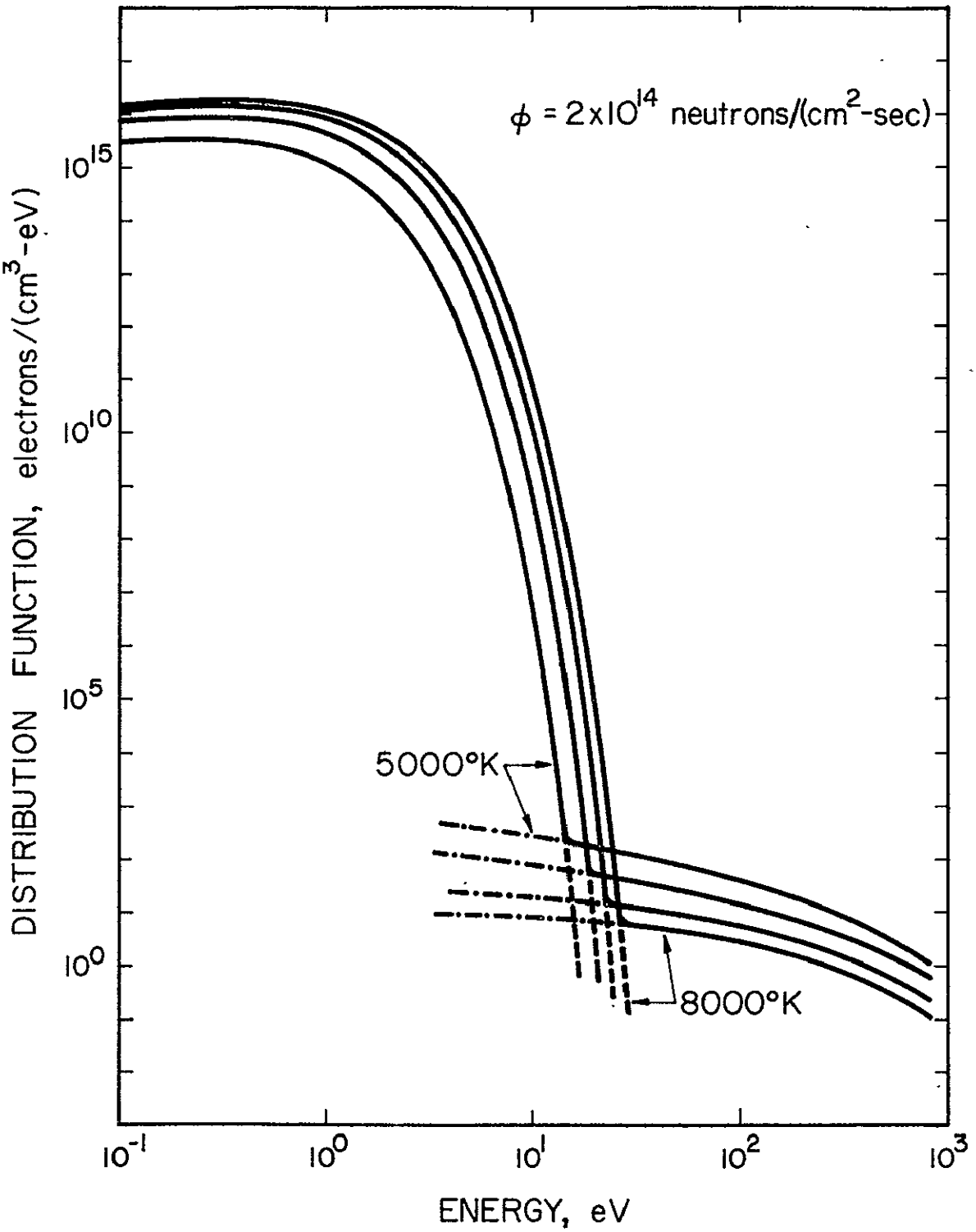

Fig. 14. Temperature dependence of distribution function is exhibited for a neutron flux of 2 x 10^{14} neutrons/(cm^2-sec) at the temperatures of 8000°K, 7000°K, 6000°K and 5000°K.

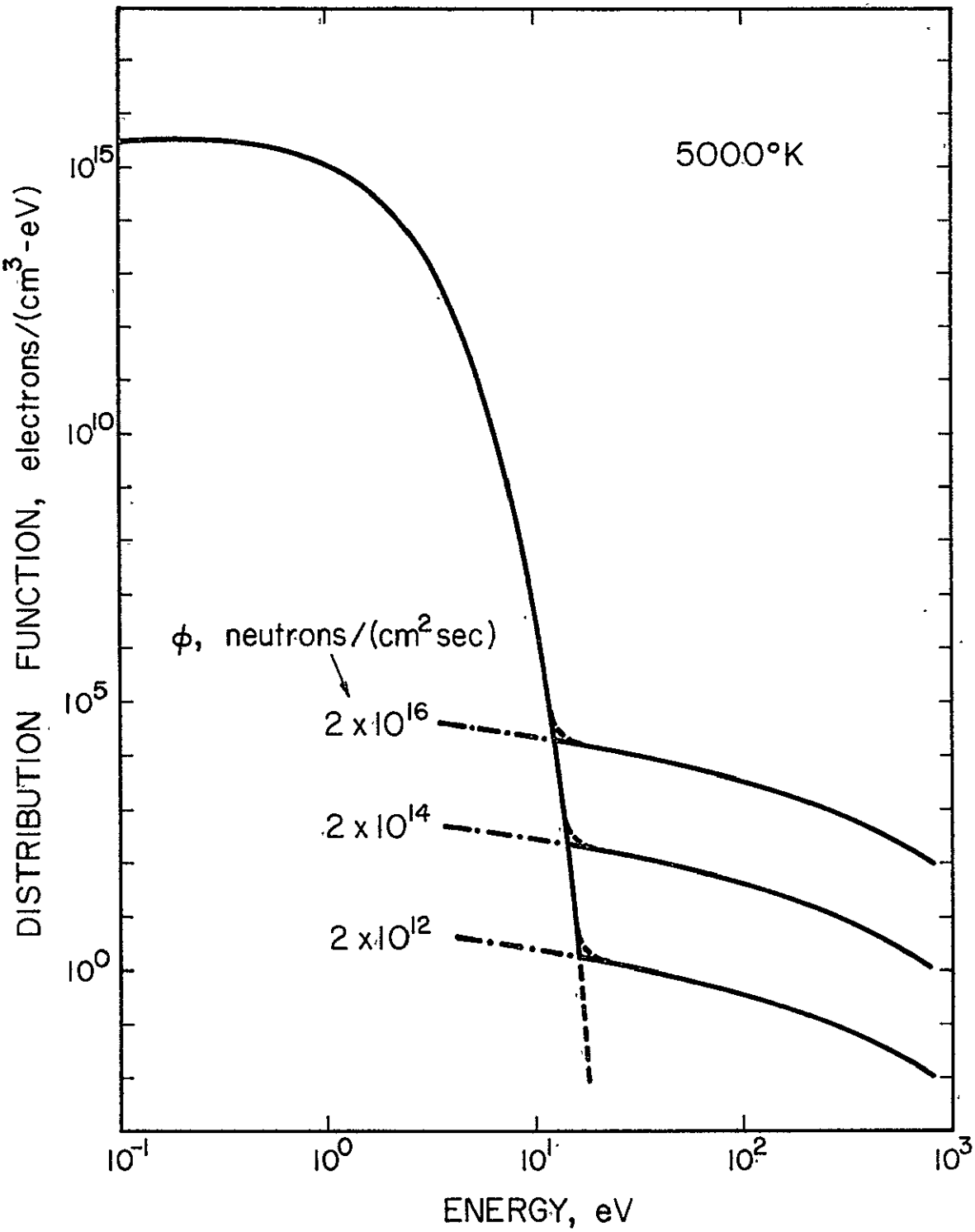

Fig. 15. Neutron flux dependence of distribution function is displayed for a temperature of 5000°K.

3. Comparison of Coulombic Energy Loss Rate Models

Previous to this, all distribution functions have been calculated with a traditional Fokker-Planck expression for the energy loss rate for Coulombic collisions. Due to the small number of electrons in a Debye sphere, collective interactions cannot be overlooked. The distribution function has been recalculated with a Coulombic energy loss rate from the unified theory[15] which incorporates both binary and collective interactions into a single theory. The results are presented in Fig. 16 for a neutron flux of 2×10^{14} neutrons/(cm^2-sec) and temperatures ranging from 8000°K to 5000°K. Also, for completeness, the range of electron energy has been extended closer than previous results to the maximum energy at which a nascent electron can be born (~2.1 keV)

Again, the general trends of the previous calculations are still preserved under a change of expressions for the energy loss rate. However, the absolute magnitude of the high-energy tail is affected by the change. This is illustrated in Fig. 17 for a neutron flux of 2×10^{14} neutrons/(cm^2-sec) and a temperature of 8000°K. (This represents the "worst" case since at higher temperatures, the Coulombic energy loss rate comprises a larger fraction of the total energy loss rate than at any other temperature considered.) In general, the energy loss rate for the unified theory is approximately 1.5 times larger than the Fokker-Planck energy loss rate, due to the additional slowing mechanisms (collective interactions and hard impact collisions) considered in the former energy loss rate. This factor decreases the distribution function by approximately a factor of 2/3 as predicted by Eq. (10).

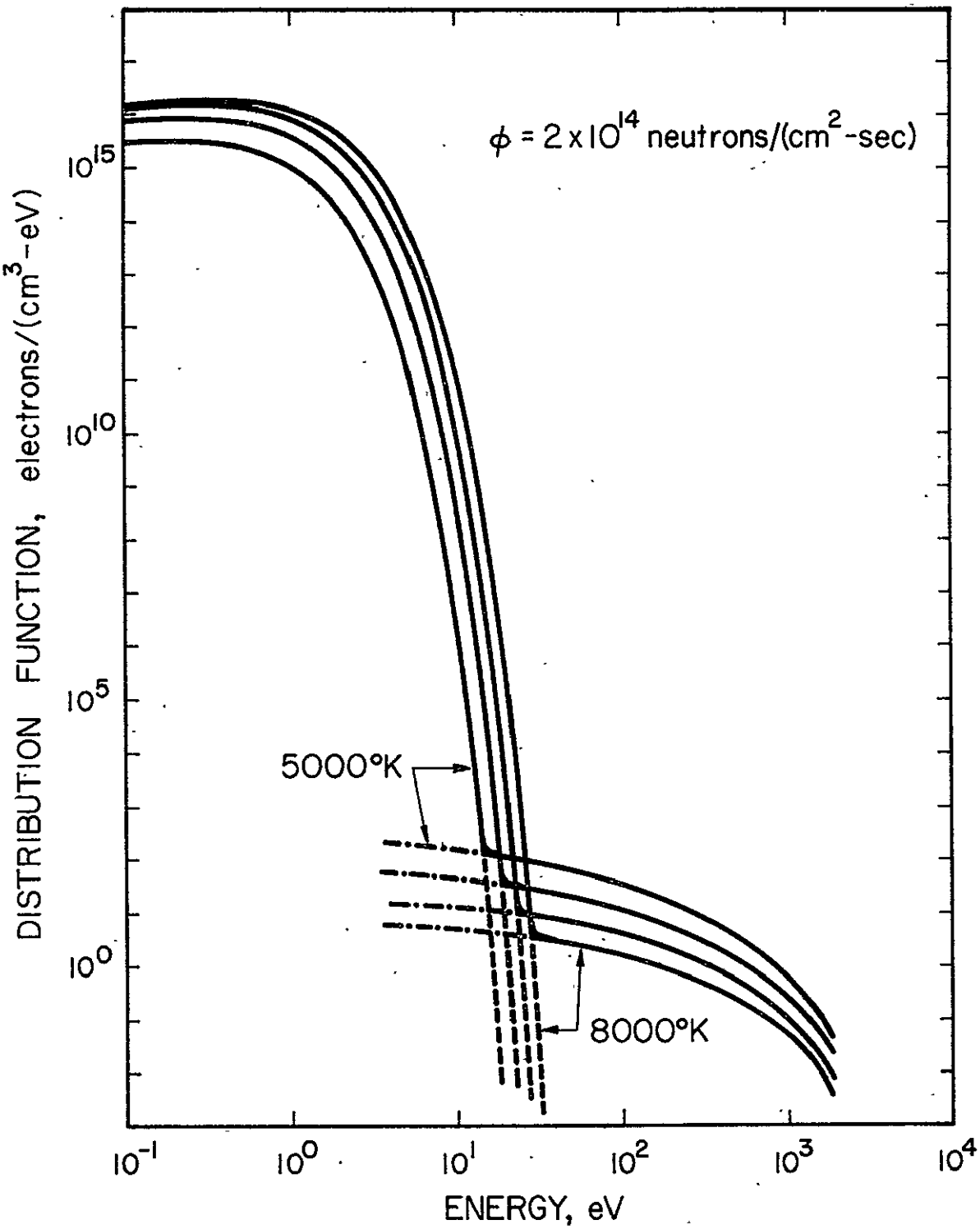

Fig. 16. Temperature dependence of distribution function is repeated as in Fig. 14, but this time using the unified slowing treatment of Coulombic collisions instead of a Fokker-Planck treatment.

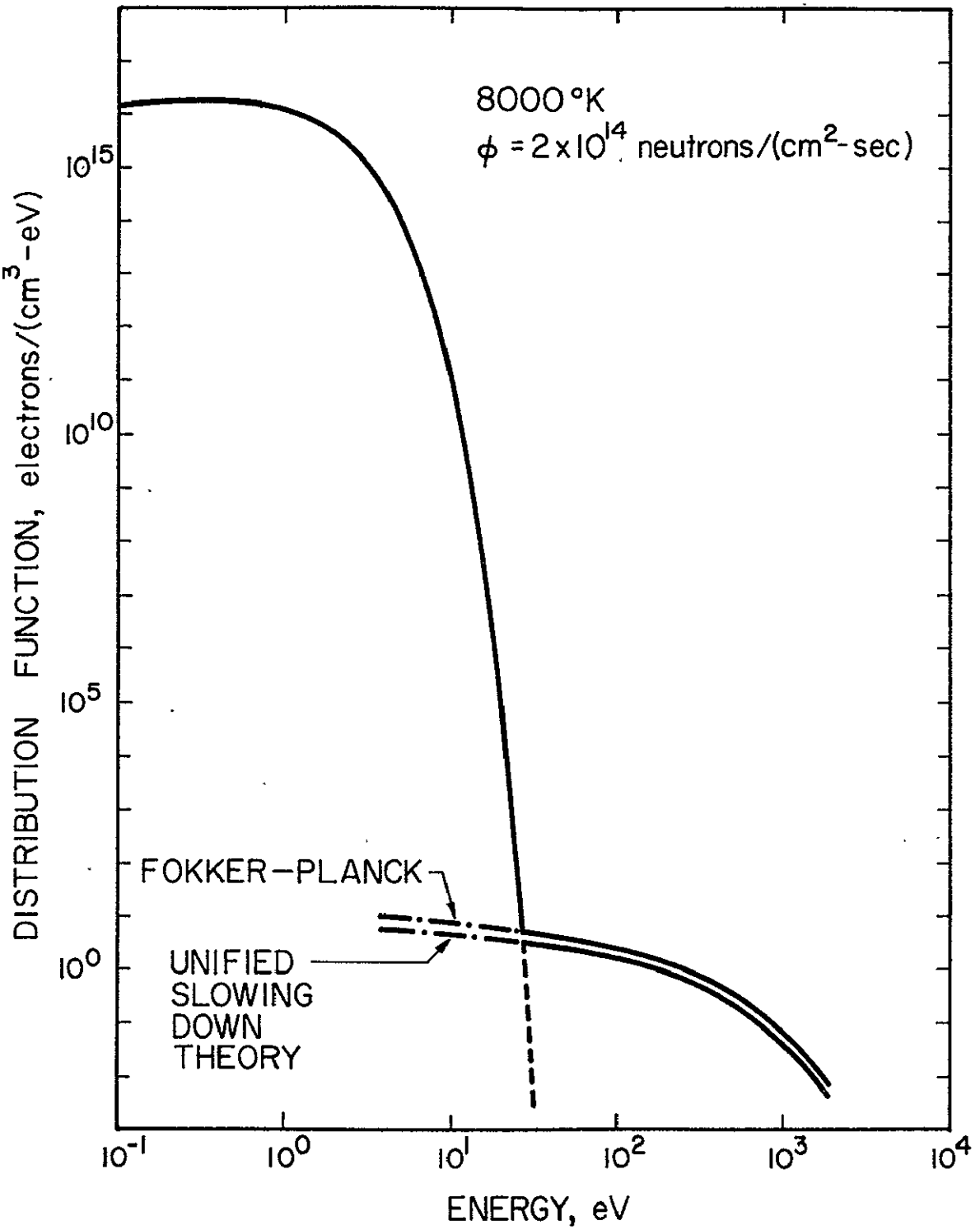

Fig. 17. Comparison of the effect of using different Coulombic slowing treatments.

F. Comparison of Methods

Although both the analytic results of Eq. (10) and the Monte Carlo simulations of Eq. (13) have been presented and common trends observed, they have not been compared with each other. In Fig. 18, a series of graphs at various temperatures and a constant neutron flux of 2×10^{12} neutrons/(cm^2-sec) illustrate the differences between the analytic (dashed line) and Monte Carlo (Δ's) results. The corresponding tail of the Maxwellian distribution (solid line) is included in each of the graphs of Fig. 18 in order to locate the intersection of the two distributions; i.e., the range of validity of the slowing down distribution.

The most significant difference in the two sets of results is the increasing gap between them with increasing temperature. This discrepancy can be explained by first observing that if both solutions were extrapolated to higher energies, eventually the analytic result would intersect the Monte Carlo result and finally lie below it, as is easily seen to be the case for 5000°K. From this, it can be concluded that at the origin or highest energy for which the nascent source exists (~2.1 keV), the analytic solution will lie closer to but always below the Monte Carlo solution, as the temperature is increased. At lower temperatures, the importance of the inelastic collisions as an energy loss mechanism increases, thereby, rendering the assumption of continuous slowing (and the analytic treatment) to be invalid at low temperatures. Although the inaccuracy may seem insignificant at the origin of the calculation (~2.1 keV), the propagation of the error amplifies the inaccuracy in a peculiar manner as described in the ensuing pages.

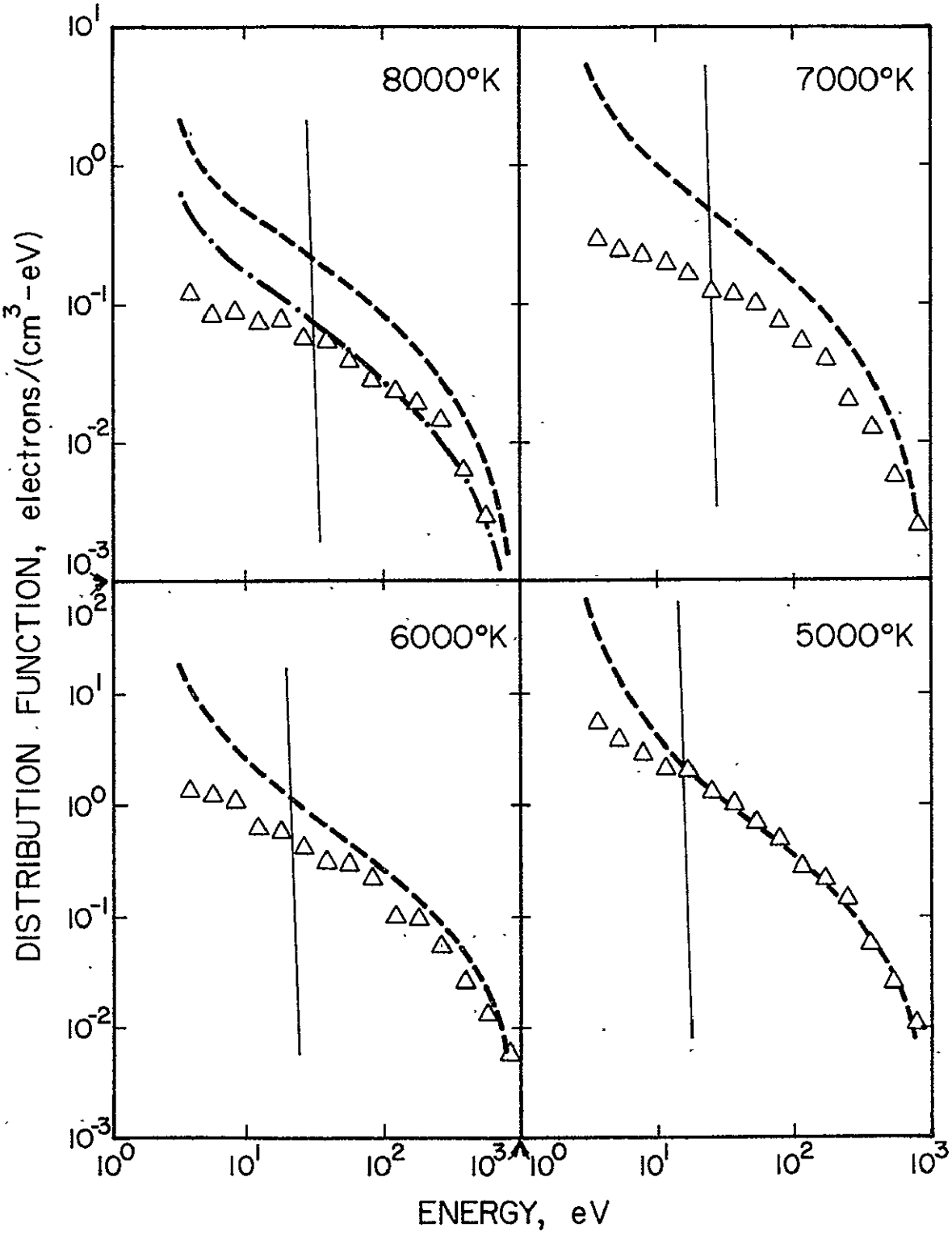

Fig. 18. A comparison of Monte Carlo results (Δ's) and analytic solution (dashed line) for various temperatures at a neutron flux of 2×10^{12} neutrons/(cm^2-sec). Maxwellian distribution is solid line. A vertically displaced analytic solution is also presented (-•-).

By examining Eq. (4), the discrepancy in the distribution function at the highest energy can be traced to the energy loss rate. Neglecting recombination, the equation can be rewritten at the point of origin of the calculation subject to the boundary condition

$$f(E+dE) = 0 \tag{39}$$

as,

$$\text{constant} \equiv S(E)\,dE = f(E)\left.\frac{dE}{dt}\right|_E \tag{40}$$

Eq. (40) demonstrates that an exaggeration of the energy loss rate will result in the underestimation of the distribution function as is observed to be the case with the analytic result in comparison to the Monte Carlo result.

The reason that the analytic method overestimates the energy loss rate lies in the continuous slowing approximation as demonstrated by the following examples.

Consider an energy cell of width ΔE located at the point of origin E + dE of the calculation, containing 100 particles distributed evenly in energy, i.e., 10 particles are in the subinterval labeled A, etc. (see Fig. 19). Furthermore, assume that an arbitrary fraction of the total particles collide per Δt, e.g., 1/10. If the average energy loss per collision is less than ΔE, e.g., $\Delta E/2$, then the number of particles which leaves the cell due to collisions according to both treatments is:

$$D_{ANALYTIC} = \frac{dE}{dt} f(E) = n\sigma V \cdot \langle \Delta E_{loss} \rangle \cdot f(E) \tag{41}$$

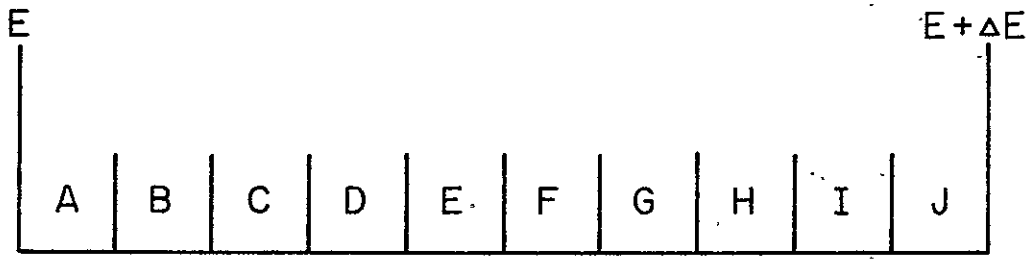

Fig. 19. Energy interval dE about E depicted at origin of calculation. The interval is subdivided into ten smaller intervals

$$= \left(\frac{1}{10\Delta t}\right) \cdot \Delta E/2 \cdot \frac{100}{\Delta E} \tag{42}$$

$$= .5/\Delta t \tag{43}$$

and,

$$D_{MONTE\ CARLO} = \frac{1}{\Delta t_A} + \frac{1}{\Delta t_B} + \frac{1}{\Delta t_c} + \frac{1}{\Delta t_D} + \frac{1}{\Delta t_E} = 5/\Delta t \tag{44}$$

where $1/\Delta t_A$ represents the one particle of the ten particles in subinterval A that collides, losing sufficient energy to escape the interval ΔE within the time Δt. Hence, both treatments yield the same result if the energy transfer is indeed infinitesimal. However, if the average energy lost per collision is larger than ΔE, e.g., $2\Delta E$, then

$$D_{ANALYTIC} = \left(\frac{1}{10\Delta t}\right) \cdot 2\Delta E \cdot \frac{100}{\Delta E} = \frac{20}{\Delta t} \tag{45}$$

and

$$D_{MONTE\ CARLO} = \frac{1}{\Delta t_A} + \frac{1}{\Delta t_B} + \frac{1}{\Delta t_c} + \ldots + \frac{1}{\Delta t_j} = \frac{10}{\Delta t} \tag{46}$$

The results of Eqs. (45) and (46) confirm that the analytic result erroneously overestimates the diffusion from the original cell by spreading out the energy loss per collision over all of the electrons within the cell, enabling more of them to leave.

At intermediate energies, both the number diffusing into an energy interval dE about E and those diffusing from the interval will be erroneously calculated in the analytic method. Because the cross sections are relatively constant and the energy loss per collision small compared to the electron energy, the errors will cancel, yielding an approximately correct slope for the distribution function at intermediate energies. This is born

out by the result at 5000°K and a renormalized result (dot-dash line) at 8000°K in Fig. 18.

At lower energies, i.e., near the point of intersection with the Maxwellian, the assumption of continuous slowing down completely breaks down. The inelastic cross-sections vary rapidly and the energy lost per excitation collision becomes a sizable fraction of the electron energy. Thus, the shapes of the Monte Carlo curves differ considerably from the analytic results in the region at, and below, the intersection with the Maxwellian. Fortunately, the worse departure occurs below the intersection where the calculation is no longer interesting.

CHAPTER IV

CONCLUSIONS

A. Review

Preliminary to the calculation of the distribution function in a uranium plasma is the assemblage of the excitation and ionization cross sections for neutral and singly ionized uranium. As no previous calculations nor measurements exist for them, the hydrogenic model of Gryzinski[16] is applied to uranium utilizing the atomic state data of Parks.[17] Furthermore, the nascent electron source, heretofore an undetermined quantity, is modeled upon a semi-empirical formulation of the fission-fragment thermalization process and the aforementioned cross-section set. Then, these calculations in conjunction with the determination of the species' densities via the Saha equations serve as the basis for the distribution function calculation.

The distribution is decomposed into two parts: a Maxwellian (valid at low energies) and a high-energy tail. The calculation of the tail is performed via two distinct methods. The first method was based upon the assumption of continuous slowing down and yielded an analytic solution from which trends could easily be predicted. The second method involved the Monte Carlo simulation of a governing equation in which the assumption of continuous slowing down had been relaxed for inelastic collisions. The second method affords a check upon the first method while serving as a powerful tool for performing detailed calculations. The disparity in the two sets of results is tracable directly to the applicability of the continuous slowing-down assumption to the inelastic collisions.

Incorporated into the Monte Carlo simulation are several noteworthy techniques developed or adapted specifically for the present case. Foremost of these are the adaptation of the rejection technique to increase the sampling efficiency and the development of the convergence propagation technique and the scheme of superimposing continuous and discrete slowing. Especially important is the latter technique as it represents the first time that Coulombic collisions are considered in irradiated plasmas which are being examined for their excitation capabilities.

In an attempt to ascertain the effect of collective interactions upon the Coulombic energy loss rate, two theories were employed. The first, the Fokker-Planck theory, is a zero order treatment in the plasma parameter g. The other, the unified theory, is a first order theory. On the basis of these two theories, it was concluded that the collective interactions were adequately incorporated into the calculation.

From the results presented here, the distribution function is concluded to be non-Maxwellian above 15 eV. Parametric studies reveal the amplitude of the high-energy tail to be linearly proportional to the neutron flux level and inversely proportional to the temperature. The degree of deviation of the high-energy tail from a Maxwellian can be gauged by the following example: for the plasma conditions of 8000°K and 2×10^{16} neutrons/(cm^2-sec), the calculated distribution induces 6×10^{14} more excitation events/(cm^3-sec) than a Maxwellian distribution.

B. Accuracy of Results

From Section F of Chapter III. it can be concluded that the Monte Carlo solution gives a much more accurate account of the collisional processes than does the analytic solution, hence, a more realistic dis-

tribution function. The Monte Carlo result can be considered statistically uncertain to within fifteen percent based upon the results of Table 3. Improved statistics can be affected primarily by increasing the number of simulation particles. However, two other factors have a greater influence upon the ultimate accuracy of the results; namely, the errors inherent in the cross-section set and the Coulombic collision treatment.

The other researchers have successfully applied the hydrogenic model of Gryzinski[16] to calculations of cross sections (e.g., Lo[22] employed the model for Helium). However, comparisons of the calculated cross section to cesium, which is similar in electronic structure, reveal that the calculated cross-section set may be somewhat low. The uncertainty involved is estimated to be a factor of 2.

The uncertainty associated with the Coulombic energy loss rate is difficult to predict. The error estimating scheme of the BBGKY hierarchy[21] is not applicable as the plasma parameter g is not small (i.e., $g \leq 5.2$). However, the ratio of the unified slowing expression (exact to order g) to the Fokker-Planck expression (accurate to order 1) is found to be only of order 3/2 in spite of the two treatments' diversity. The Fokker-Planck expression depicts a test particle's interactions with the background within the annulus defined by $b_o < r < \lambda_D$, where b_o = and λ_D are the close impact parameter and the Debye length, respectively; while the unified theory depicts those interactions within the annulus $0 < r < \infty$. Because each treatment is so different, yet their results are in good agreement, it seems reasonable to conclude that the actual energy loss rate is close to that predicted by these two theories. If additional correlation (or collective) effects enter, the energy loss rate would be even larger than

that predicted by the unified theory. A liberal estimate of the energy loss rate would be a factor of 5 larger than the Fokker-Planck result.

The uncertainty associated with the inelastic cross-sections can increase the distribution by a factor up to two particularly at high T. Similarly, the Coulombic energy loss rate could possibly introduce a factor of two in the opposite direction also preferentially at high T. Then, the effects tend to cancel, and the final result can be more accurate than either of the components of the calculation, i.e., the distribution functions reported here (e.g., Figs. 14 and 15) are uncertain to within a factor estimated to be considerably less than two.

C. Implications to Uranium Plasma Program

The results presented in Section E of Chapter II and III clearly demonstrate the distribution function to be non-Maxwellian. The importance of this is partially lost since the bulk of the excitation out of the ground state is done by electrons below the intersection in energy of the tail and the Maxwellian. For 8000°K, a Maxwellian distribution will cause approximately 1.4×10^{24} excitations/(cm^3-sec). Above 22 eV, however, the Maxwellian will cause 3.2×10^{13} excitations/(cm^3-sec) while the high-energy tail will cause 6.6×10^{14} and 3.9×10^{13} excitations/(cm^3-sec) for neutron fluxes of 2×10^{16} and 2×10^{14} neutrons/(cm^2-sec), respectively. These excitation rates may not produce inversions of the excited state densities in a uranium plasma. However, if the plasma were seeded with a species with a high threshold energy for the first excited state, e.g., helium, then ideal conditions exist for predominately exciting the helium with the non-Maxwellian tail. Then, clearly, the significance of the high-energy tail is determined by the type of interaction under consideration.

D. Future Work

1. Further Applications and Development of Code

The presence dependence of the distribution should be investigated. Crucial to this investigation is the size of the perturbation to the Saha densities caused by the fission-fragments. The changes in the densities of the various plasma species will determine if the distribution can be extrapolated from the results presented here. If not, the calculations must be repeated with the appropriate densities (and corresponding temperatures).

An additional effect that should be incorporated is spatial diffusion. This effect is neglected in this work as the projected size (1 meter) of the device containing the uranium plasma makes the plasma an infinite one. The electrons in the high-energy tail will preferentially leak out from the system, thereby decreasing the perturbation of the high-energy tail on the Maxwellian.

One must not neglect the need for implementing improved inelastic cross sections as they become available. Also, the Coulombic interactions are in need of a model which can more precisely describe the interactions under the unique plasma parameters incurred. By far, these two aspects are most in need of improvement.

2. Analysis of Other Plasmas

From the conclusions reached in section B, the code needs to be expanded in order to accommodate the presence of seed species as well as buffer gases. These additional species introduce important factors in the calculation of a distribution function in a working uranium plasma and the initially planned experiments. Their presence will dilute the

electron source and in the case of the seed gas decrease the stopping power of the plasma. It is difficult to judge a priori if these opposing trends will cancel each other. Furthermore, the introduction of molecules, e.g., UF_6 into the plasma will complicate the calculation of energy loss rates with the introduction of vibrational and rotational excitation processes. The ease with which these excitation processes occur will increase the energy loss rate, decreasing the high-energy tail. A more detailed analysis is possible through the adaptation of existing treatments of electron slowing via molecular excitation collision.[45]

The code might also be applied to other plasmas with a distributed source of nascent electrons. The plasmas will have to be restricted to those which satisfy the assumption that the high-energy tail is only a perturbation to a Maxwellian distribution. This excludes plasmas with electric fields wherein the bulk of the plasma is describable by a Druyvestyen distribution.

APPENDIX A

ENERGY LOSS RATES

1. Fokker-Planck

For the majority of the calculations reported in Chapters II and III, a traditional Fokker-Planck expression for the Coulombic energy loss rate was employed. The limited applicability of the Fokker-Planck expression due to the small number of electrons within a Debye sphere was pointed out previously in Chapter I. However, the expression was used in spite of the expansion factor g not being negligible compared to one, following the lead of others in applying the expression under similar circumstances, e.g., in MHD calculations of conductivity[46] and in modeling afterglows.[29] The precise equation utilized is:

$$\frac{dE}{dt} = 4\pi q^2 \sum_{s=1}^{n} \frac{n_s e_s^2}{m_s v} F_s\left(\frac{v}{v_s}\right) \ln\left\{1 + \frac{\left(v^2 + \frac{2kT_s}{m_s}\right)^2 m^2 m_s^2}{g^2 q_s^2 \lambda_D (m^2 + m_s^2)}\right\} \quad (47)$$

where n_s, m_s, q_s, and T_s denote the background species s's density, mass, charge, and temperature; m, q, and v denote the test particle's mass, charge, and velocity; and the Debye length is λ_D. The function F_s appearing in Eq. (47) is defined as:

$$F_s(U) = \frac{2}{\pi^{1/2}} \left\{ \int_0^1 \exp(-U^2 x^2)\, dx - \left(1 + \frac{m_s}{m}\right) \exp(-U^2) \right\} \quad (48)$$

Calculations of the energy loss rate as prescribed by Eq. (47) appear in Figs. 20 and 21. A discussion of the results appears in the next section.

2. Unified Theory

In Chapter I, the speculation that collective interactions play a dominant role in the slowing of energetic electrons leads to the need to

consider a higher order kinetic equation, i.e., the Lenard-Balescu[35] equation. The traditional treatments of charged particle slowing in the Lenard-Balescu or wave theory, e.g., Sigmar and Joyce,[47] introduce a cutoff to eliminate a singularity in the analysis. The uncertainty associated with the introduction of a cutoff, especially under the plasma conditions present in the uranium plasma, render these treatments inappropriate. A theory which is independent of a cutoff was developed by Kihara and Aono.[15] Since this theory depicts the full spectrum of interactions, i.e., from collective interactions to close impact collisions, it is exact to order g. Then, through its implementation, the effect of neglecting collective interactions can be gauged.

The theory of Kiharo and Aono or the unified theory is based upon the observations of Hubbard[36] that the divergences appearing in traditional wave and impact theories could be made to cancel each other. Symbolically, this can be written as

$$X'_{exact} = X_{impact} + X_{wave} - X_{dual} \tag{49}$$

where X denotes a reaction rate, e.g., the n^{th} moment $\frac{<\Delta v^n>}{\Delta t}$, in either the close impact or wave theory. The subtrahend X_{dual}, an expression which neglects the effect of collective interactions and the effect of orbital curvatures, is responsible for the cancellation of the divergence in both these theories. Although Hubbard's formulation also includes the full spectrum of interactions, the resulting energy loss rate is not independent of cutoffs.

The prescription for calculating a relaxation rate in the unified theory is dependent upon casting a relaxation rate in both the wave theory

and impact theory in the following forms

$$X_{wave} = \int_{k>0} dk\, K(k) \tag{50}$$

and

$$X_{impact} = \int_{b>0} db\, B(b) \tag{51}$$

where k is the wave number in the wave theory and b is the impact parameter in the impact theory. The theory of unification then states that the non-diverging relaxation rate is given by

$$X_{exact} = \int_0^\infty B(b) \exp(-\tfrac{1}{2} b^2/b_o^2)\, db + \int_0^\infty K(k) \exp(-\tfrac{1}{2} k^2 b_o^2)\, dk \tag{52}$$

where b_o is an intermediate length, less than the Debye length and greater than the close impact radius. A relaxation rate calculated according to Eq. (52) is independent of the intermediate length b_o.

As an exercise in the unified theory, Itikawa and Aono[37] calculated the relaxation of a test particle of arbitrary velocity in a plasma. Their result is of the form

$$\frac{dE}{dt} = 4\pi q^2 \sum_{s=1}^{n} \frac{n_s e_s^2}{m_s v_s} \left\{ F_s\left(\frac{v}{v_s}\right) \ln\left(\frac{4\mu_s T_s}{\gamma |e_s q| m_s k_s}\right) + G_s\left(\frac{v}{v_s}\right) \right\} \tag{53}$$

where $\ln\gamma = 0.5772$, $v_s = \sqrt{\frac{2kT_s}{m_s}}$, and $\mu_s = \frac{m_s m}{(m_s+m)}$. The term G_s contains the Coulomb logarithm dependence upon the velocity of the test particle. The exact form of G_s is[38]

$$G_s(U) = 2U^2\left(1+\frac{m}{m_s}\right)\tilde{G}(U) - \tilde{\Phi}(U) - \frac{m}{m_s} g_{ss'}(U) + \varphi_{ss'}(U) \tag{54}$$

where $u_s = v/v_s$ and

$$\tilde{G}(U) = 2\,G(U) + \frac{\tilde{\Phi}(U) - U\,\tilde{\Phi}'(U)}{2U^2} \tag{55}$$

$$G(U) = \frac{\Phi(U) - U\,\Phi'(U)}{2U^2} \tag{56}$$

$$\Phi(U) = \frac{2}{\sqrt{\pi}} \int_0^U e^{-x^2}\, dx \tag{57}$$

$$\tilde{\Phi}(U) = \frac{2}{\sqrt{\pi}}\, U \int_0^\infty dx \int_{-1}^{1} dt\; x \ln x^2 \cdot e^{-(U^2 + x^2 + 2xUt)} \tag{58}$$

$$g_{ss'}(U) = \frac{4}{\sqrt{\pi}} \int_0^U dx\; x^2 e^{-x^2} C_{ss'}(x) \tag{59}$$

$$\varphi_{ss'}(U) = \frac{2}{\sqrt{\pi}}\, U^2 e^{-U^2} C_{ss'}(U) \tag{60}$$

$$C_{ss'}(U) = \frac{1}{4} \ln\left(A_{ss'}^2(U) + B_{ss'}^2(U)\right) + \frac{A_{ss'}(U)}{2|B_{ss'}(U)|} \left\{ \frac{\pi}{2} - \tan^{-1} \frac{A_{ss'}(U)}{|B_{ss'}(U)|} \right\} \tag{61}$$

$$A_{ss'}(x) = \xi(x) + \beta_{ss'}\, \xi(\alpha_{ss'} x) \tag{62}$$

$$B_{ss'}(\chi) = \eta(\chi) + \beta_{ss'}\,\eta(\alpha_{ss'}\chi) \tag{63}$$

$$\xi(\chi) = 1 - 2\chi e^{-\chi^2}\int_0^{\chi} e^{t}\,dt \tag{64}$$

$$\eta(\chi) = \sqrt{\pi}\;\chi\; e^{-\chi^2} \tag{65}$$

$$\alpha_{ss'} = \frac{v_s}{v_{s'}} = \sqrt{\frac{T_s\, m_{s'}}{T_{s'}\, m_s}} \tag{66}$$

$$\beta_{ss'} = \left(\frac{k_{s'}}{k_s}\right)^2 = \frac{g_{s'}\, T_s}{g_s\, T_{s'}} \tag{67}$$

Due to the complexity of Eq. (54) in its entirety, a more tractable expression for G_s, as developed by Perkins,[39] was substituted in place of the exact expression. Perkins' expression [Eq. (68)] is based upon the asymptotic behavior of Eq. (54) i.e.,

$$G_s(v) = F_s(v)\; g_s \tag{68}$$

where

$$g_1 = 3\ln\frac{v}{v_1} + 1/2 \qquad g_2 = 2\ln\frac{v}{v_2} \quad v > v_1 \tag{69}$$

$$= \ln 2 - C \qquad = 2\ln\frac{v}{v_2} \quad v_1 > v > v_2 \tag{70}$$

and the subscript 1 denotes the electrons and the 2 denotes the ions. Some error is introduced into the energy loss rate when Eq. (68) is em-

ployed as v approaches v_2. However, this error can be gauged to be negligible for the electron energies considered through an analogous comparison of a Butler and Buckingham[40] type expansion to the Fokker-Planck expression.

The Coulombic energy loss rates predicted by both the Fokker-Planck theory and the unified theory appear in Figs. (20) and (21) for plasma temperatures of 5000°K and 8000°K respectively. The disparity between the two theories grows as the electron energy decreases until a maximum is reached between 2 and 3 eV. This effect can be attributed largely to the better coupling of the electrons with plasma waves as the electrons approach the wave velocity. By increasing the temperature, the disparity is observed to increase only slightly. This is the result of the increased presence of collective interactions due to a further penetration into the classical collective plasma region of Fig. 2.

The history of a test electron as it slows down in each of the slowing theories is displayed in Figs. 22 and 23. The disparity in the slowing profiles is attributed to the increased stopping power in the unified theory due to the presence of collective interactions. A measure of this disparity is the thermalization time, defined here to be the time to slow from 1 keV to 1 eV. From Figs. 22 and 23, the Fokker-Planck theory is observed to yield a thermalization time approximately 1.6 times larger than that predicted by the unified theory. The factor 1.6 represents a first approximation to the inaccuracy introduced by the small number of particles within a Debye sphere. Although this degree of inaccuracy would seem undesirable, the inaccuracy associated with the inelastic collisions, which are equally important in determining the total energy loss rate, is

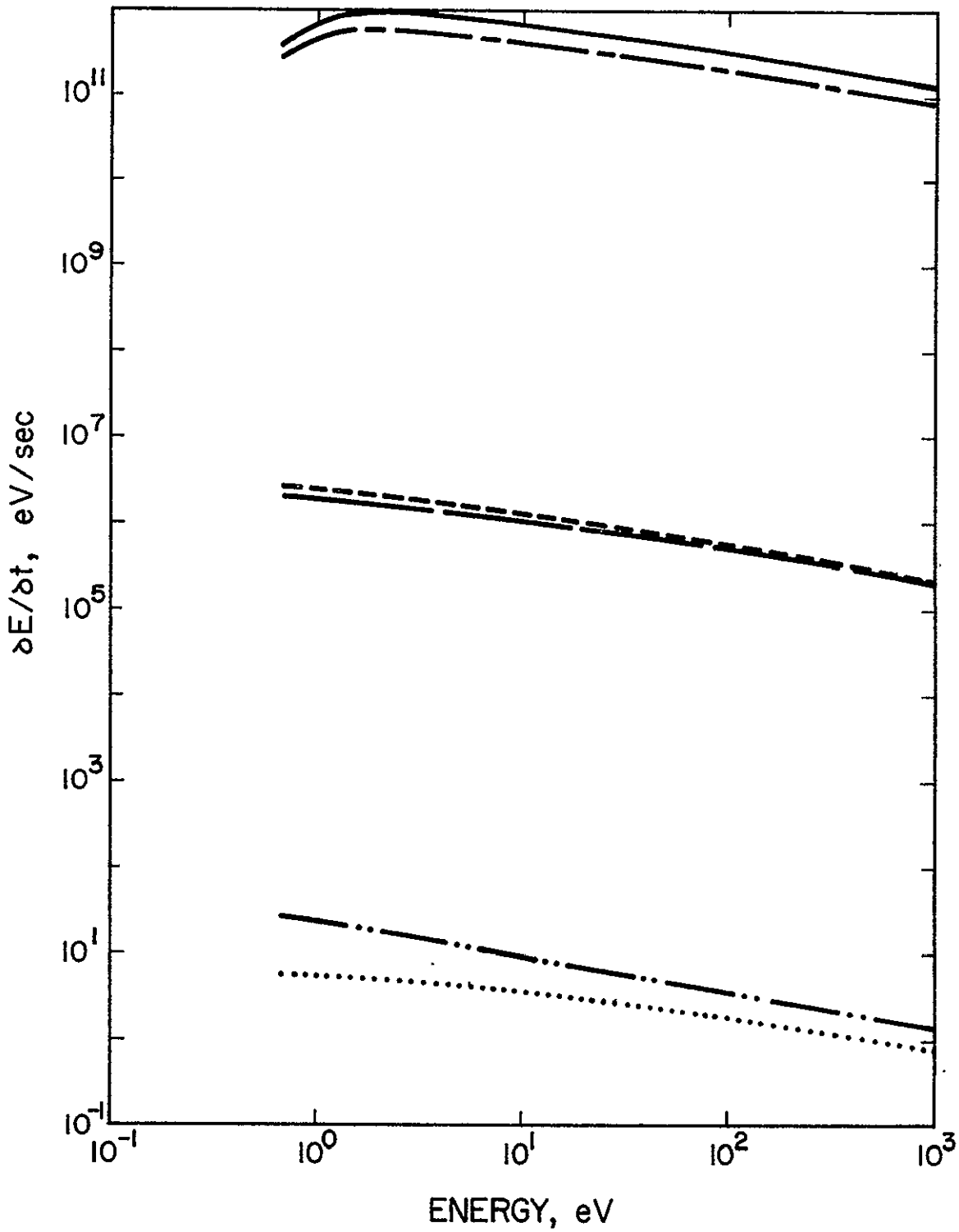

Fig. 20. The Coulombic energy loss rates for an electron slowing off of the various plasma species and the total loss rate versus energy for both Fokker-Planck (FP) and Unified Theories (UT) in a 5000°K plasma. The total and electron energy loss rates are denoted by (– – –)FP and (-) UT. The singly ionized uranium energy loss rate is denoted by (– –)FP and (----)UT, while the doubly ionized uranium energy loss rate is given by (•••••)FP and (-•••-)UT.

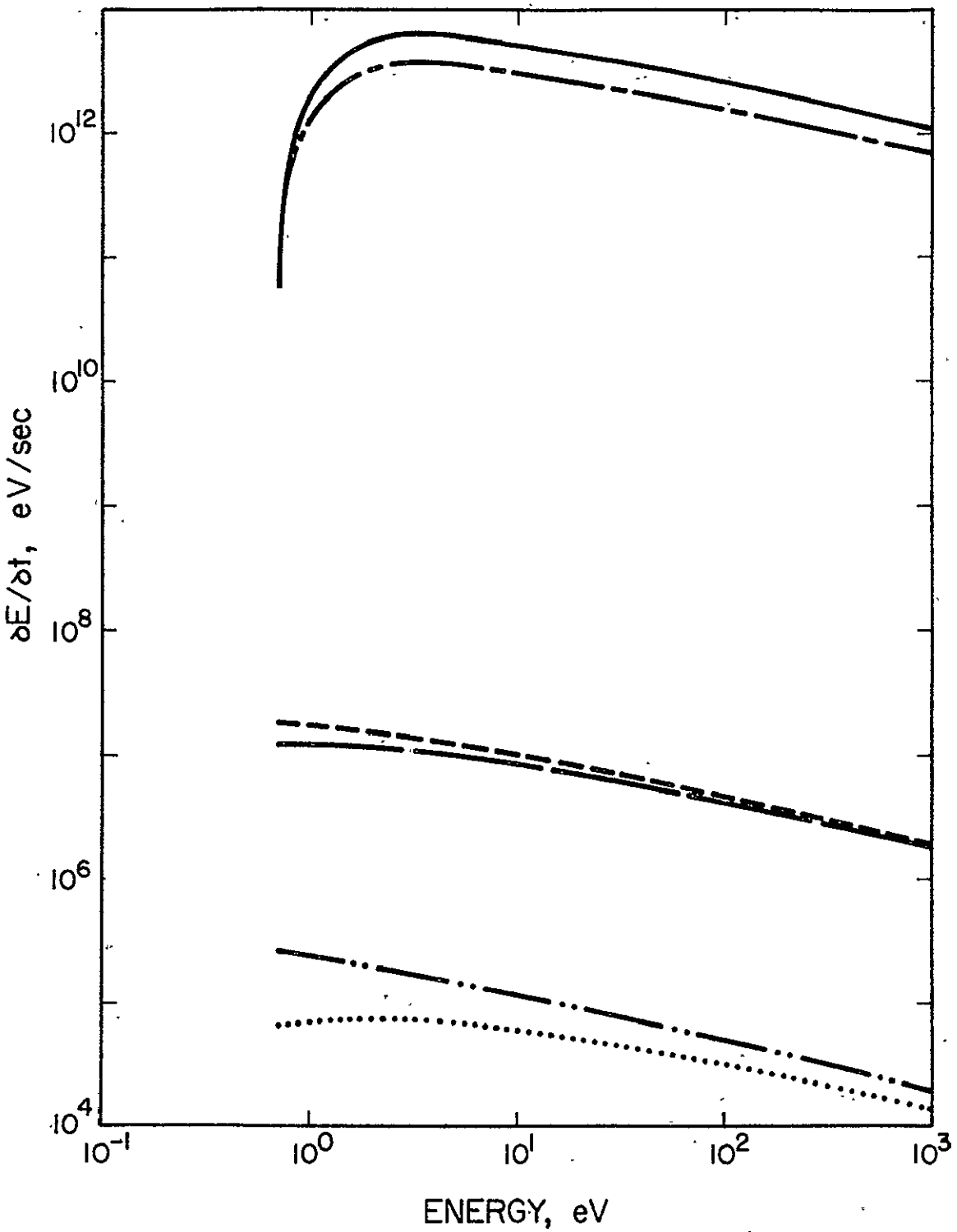

Fig. 21. The Coulombic energy loss rates for an electron slowing off of the various plasma species and the total loss rate versus energy for both Fokker-Planck (FP) and Unified Theories (UT) in a 8000°K plasma. The total and electron energy loss rates are denoted by (— - —)FP and (-)UT. The singly ionized uranium energy loss rate is denoted by (— —)FP and (----)UT, while the doubly ionized uranium energy loss rate is given by (••••)FP and (-••-)UT.

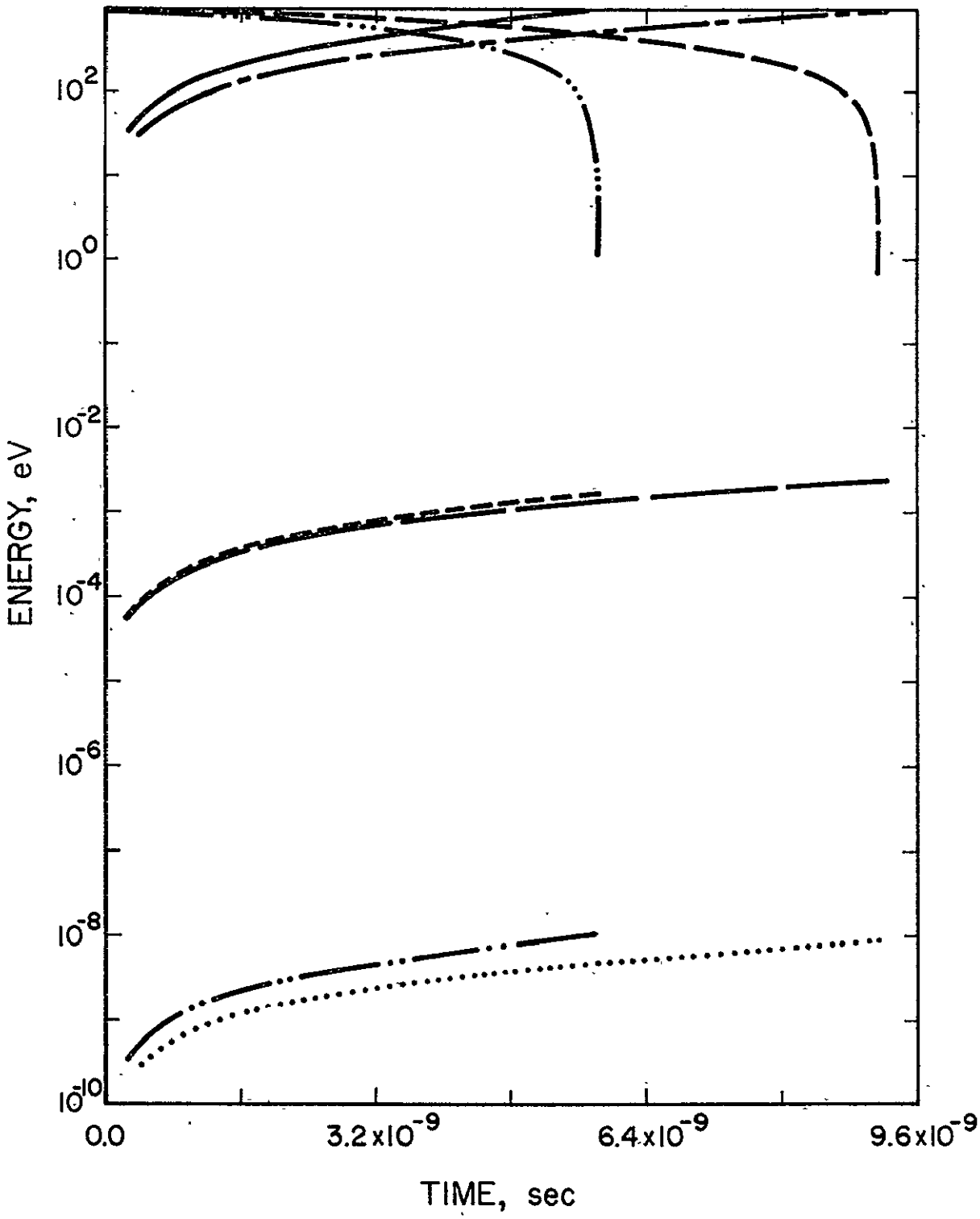

Fig. 22. The energy of a test electron is plotted versus time as it slows according to FP and UT theories in a 5000° plasma denoted by (--) and (-•••-) respectively. The energy gained by each of the plasma species is also plotted versus time with the same delineation of species and theories as in Fig. (20).

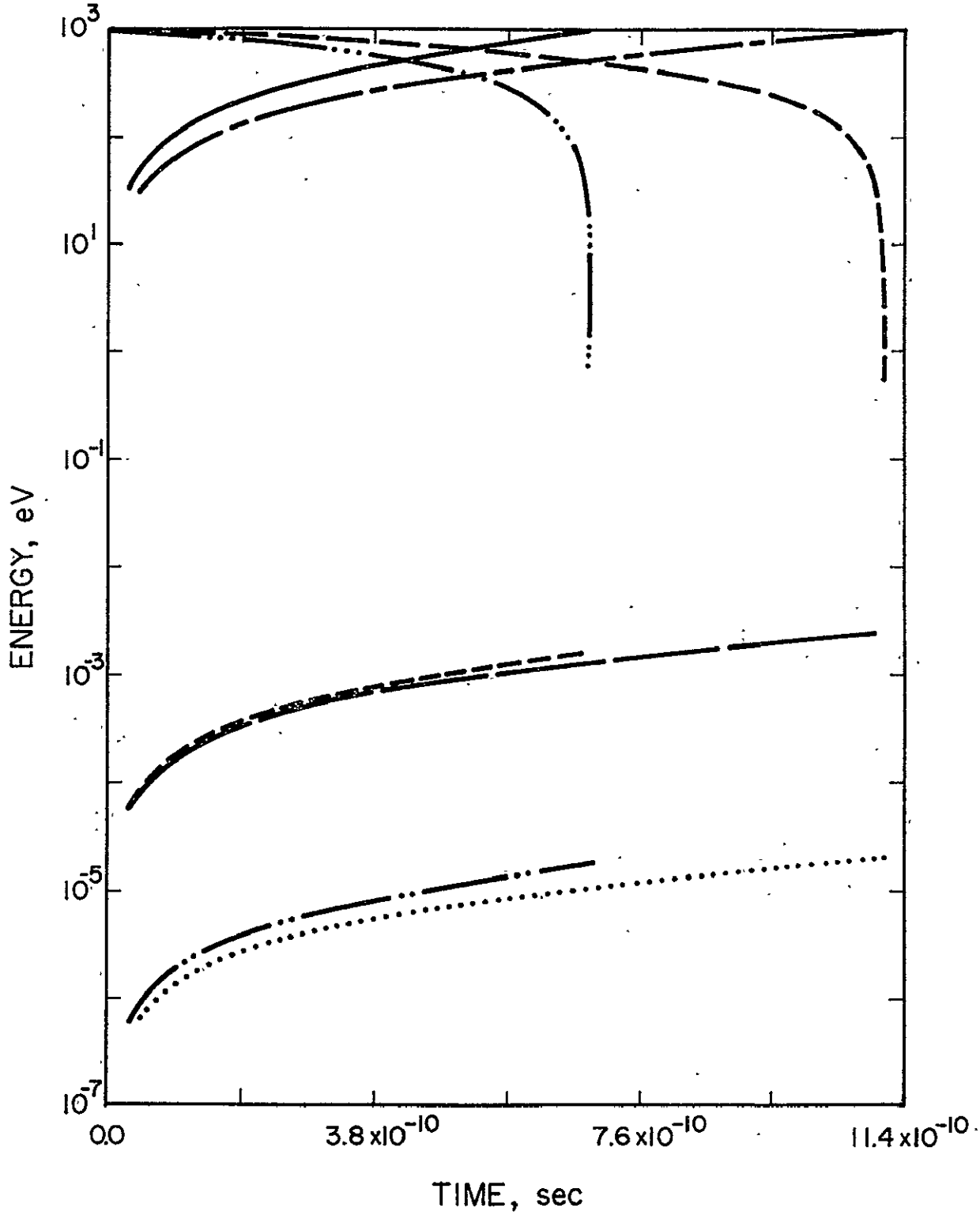

Fig. 23. The energy of a test electron is plotted versus time as it slows according to FP and UT theories in a 8000°K plasma denoted by (--) and (-•••-) respectively. The energy gained by each of the plasma species is also plotted versus time with the same delineation of species and theories as in Fig. (21).

even larger. Then, for the present calculation, the agreement between the unified theory and the Fokker-Planck theory is satisfactory

APPENDIX B

CROSS SECTIONS

Appearing in Fig. 24, are the ionization and excitation cross sections for electron bombardment of neutral, singly, and doubly ionized uranium. The cross sections have been calculated from formulae based upon a symmetrized version of the Gryzinski model as reported by Burgess and Percival,[16] implementing the ionization and excitation data of Parks, et al.[17] Because of the lack of a well-defined state corresponding to the ionization potential of the various uranium species, it has been assumed that a limited number of the outermost electrons, usually 8 or less, participate in both ionization and excitation processes. The excitation cross section represents a sum of cross sections for transitions from the ill-defined ground state, consisting of any of the outermost electrons employed in the representation of a state corresponding to the ionization potential, to a multitude of excited states, 27 total excited states for each species (see Table 4). The transitions are governed by the selection rule $|\Delta\ell| = 1$. The multiplicity of the allowable transitions eliminates the resonance behavior typically exhibited in excitation cross sections, e.g., cesium.[41]

As can be seen from Fig. 24, the cross sections exhibit an abrupt rise at the threshold energy as is characteristic at the onset of a quantum mechanical process. For energies below the threshold, the cross sections approach zero, but because it is not of immediate interest, this threshold region has not been explored in greater depth. The appearance of discontinuities in the slopes of the cross-sections are indicative of one electronic state's participation in an event being overshadowed by

SPECIES / STATE	U		U^+		U^{++}	
	E	ℓ	E	ℓ	E	ℓ
EXCITED STATES	.14	5	.54	5	1.22	5
	.16	5	.67	5	1.49	5
	.22	5	.86	5	1.90	5
	.22	4	.87	4	1.90	4
	.27	5	1.11	5	2.04	3
	.27	4	1.13	4	2.44	5
	.37	3	1.31	3	2.58	4
	.38	5	1.49	5	2.72	3
	.38	4	1.49	4	3.40	5
	.50	2	1.77	2	3.40	2
	.52	3	1.77	1	3.53	4
	.54	5	1.90	3	3.53	1
	.54	4	2.04	0	3.80	3
	.54	1	2.17	5	3.94	0
	.65	0	2.17	4	4.89	5
	.76	2	2.44	2	4.89	2
	.80	3	2.72	1	5.16	4
	.84	1	2.85	3	5.16	1
	.86	4	3.12	0	5.70	3
	1.07	0	3.40	4	5.98	0
	1.36	2	4.07	2	7.73	2
	1.49	3	4.35	1	7.77	4
	1.51	1	5.57	0	8.28	1
	2.04	0	5.84	3	9.86	0
	3.80	2	7.88	3	9.98	3
	4.89	1	8.83	2	14.94	2
	-	-	10.19	1	16.30	1
IONIZATION STATES	4.48	2	13.72	0	20.10	4
	7.88	0	17.65	4	41.69	1
	30.69	1	37.48	1	52.42	1
	41.83	1	48.62	1	73.47	0
	63.15	0	70.07	0	127.38	2
	107.28	4	124.94	2	-	-
	118.01	2	-	-	-	-

Table 4. The uranium states and their corresponding quantum numbers employed in the cross-section calculation (after Parks, et al.[17])

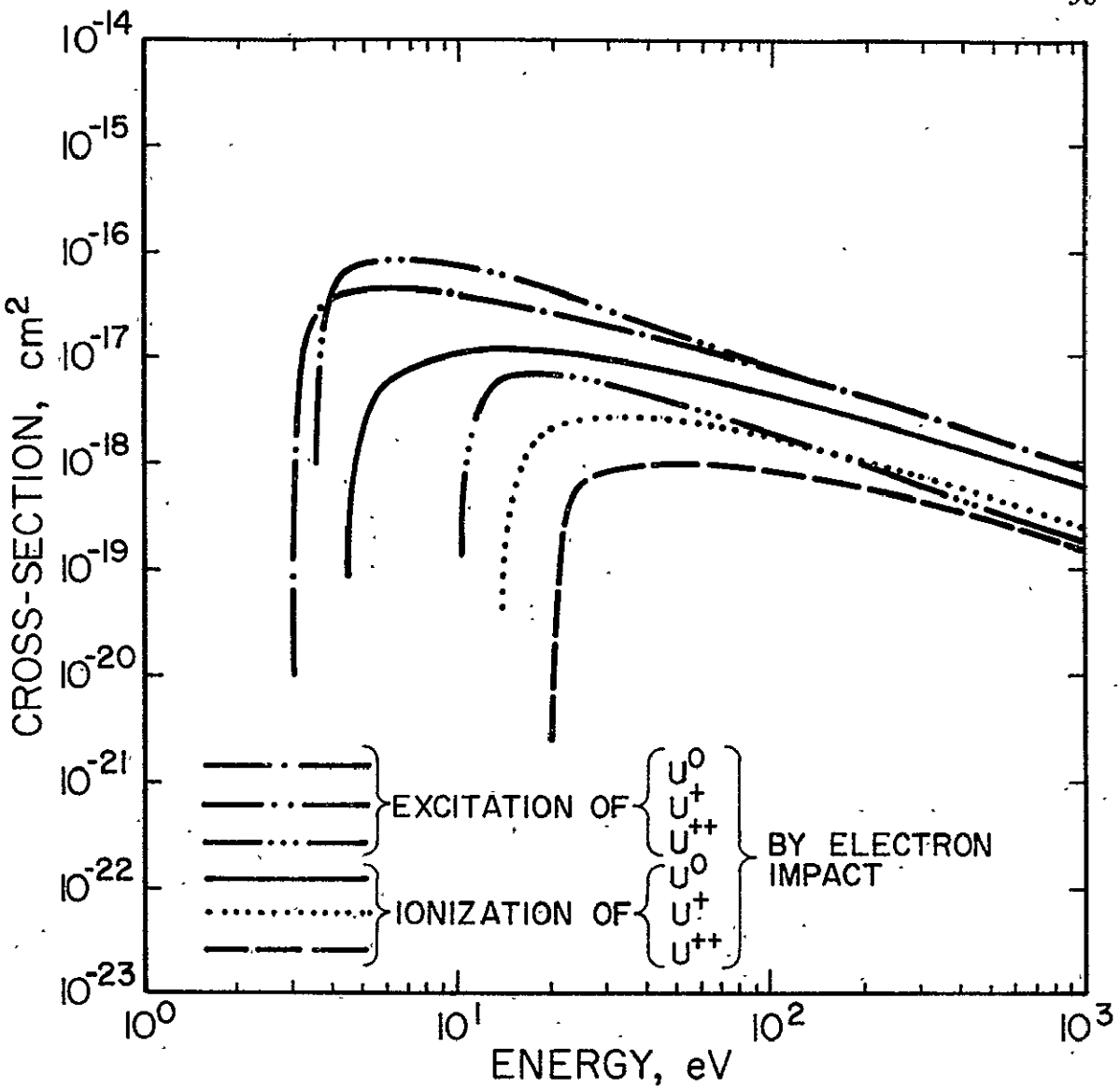

Fig. 24. The ionization and excitation cross sections for U, U^+, and U^{++} versus energy.

C-2

another state; e.g., the discontinuity in the slope of the U^+ ionization cross section at 18 eV represents the appearance of an inner-electron ionization process which, at high energies, overshadows the ionization of the outer-most electron. At very large energies, the fine structure of the atom gives way to an 1/E energy dependence.

The excitation cross sections are found to be larger in magnitude than the corresponding ionization cross-sections. A similar trend is observed for cesium[41] which is quite similar in electronic structure. These observations can be attributed to a cross section, in general, being inversely proportional to the energy transferred. Then, the smaller energy transfer afforded by excitation collisions result in the increased probability of their occurance over ionization collisions.

A comparison of the magnitudes of the uranium cross sections presented here to cesium ionization and excitation cross sections[41] reveals that the uranium cross sections are smaller by an order of magnitude than the cesium cross sections which are measured accurate to within a factor of 2. This trend can be explained by examining their ionization potentials; namely, I_{Cs} = 3.89 eV as opposed to 6.22 eV for neutral uranium. The similar electronic structure of the two elements as well as the relatively close proximity of their ionization potentials suggest that the uranium cross sections should be somewhat smaller due to uranium's larger ionization potential (implying a larger energy transfer). This is in qualitative agreement with the present results. However, a comparison with helium cross sections[42] reveals the uranium cross sections to differ from the cesium cross sections by a wider margin than anticipated. The uranium cross sections are an order of magnitude lower than cross sections of

cesium and other elements with similar ionization potentials. Yet, the Gryzinski model was found to be inaccurate by at most a factor of two for helium.[22] Then, without further experimental data for guidance, a crude estimate of the error introduced by applying a hydrogenic model for cross sections to uranium can be ascribed to be a factor of two too low.

The ability of an ionized particle to focus approaching electrons, thereby, enhancing the cross section is also taken into account in these calculations in the manner prescribed by Burgess and Percival. This effect can best be seen by comparing the excitation cross section of U and U^+. One would expect the tighter bound electrons of U^+ to be harder to excite. However, the charge on U^+ not only draws in electrons that would normally pass on by, but it also gives them additional energy as they are accelerated in the potential field. This more than compensates for the tighter shell structure of U^+.

APPENDIX C

COMPUTER CODE

A digital computer code was developed to solve Eq. (26) employing the simulation technique described in Section C of Chapter III. The simulation technique was augmented by various variance reduction techniques to enhance the rate of convergence of the solution. In order to further reduce computational time, several computational "tricks" were employed. All of which are to be described in the ensuing pages.

The computer code can best be described through references to the flow chart in Fig. 25. Although the flow chart provides an over-simplified view of the program, the spirit of the calculation is preserved by it. Numerals have been placed adjacent to the flow diagram to aid in the identification of various sections of the code. Let us begin to follow the flow of the logic with Section

Input

The first section contains the input parameters. One such parameter is the random number starter. By altering this number, a different random number string is used as the basis of the Monte Carlo simulation. Such freedom is essential to statistical testing of the results.

The plasma properties such as density, temperature, neutron flux, and identification of background species through mass and charge constitute a second set of input parameters. These parameters permit parametric studies of the effect of the plasma environment upon the relaxation of nascent electrons into a Maxwellian distribution. Some of the parameters are correlated, such as temperature and density. These parameters must be self-consistent upon input as they determine into which

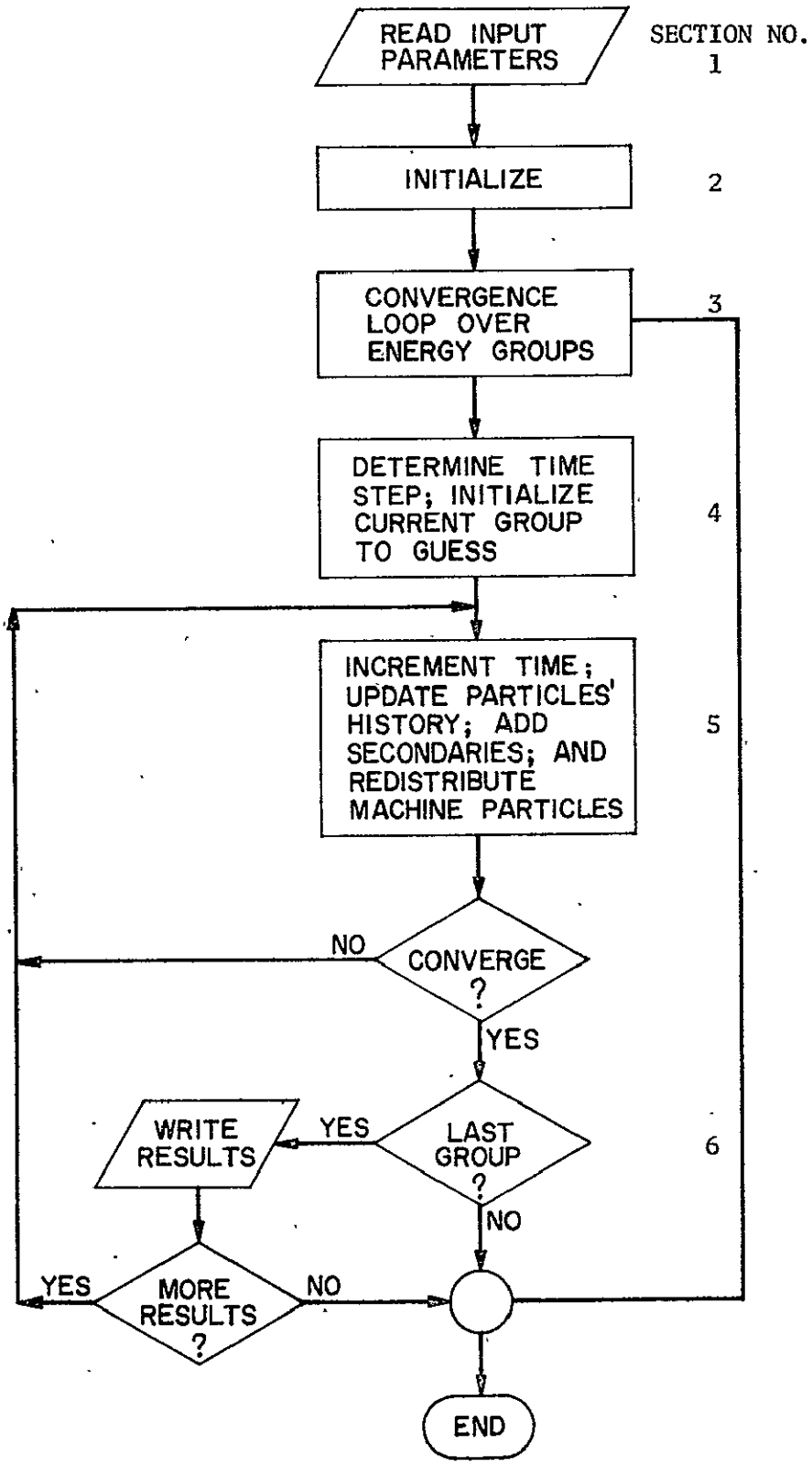

Fig. 25. Flow Chart of Monte Carlo Code.

specific target Maxwellian the nascent electrons will relax. Although the plasma species can be changed through the input data, the change is not complete without providing a new subroutine containing the appropriate cross-section set.

Another input parameter consists of an initial guess for the distribution function. Previous attempts at Monte Carlo simulations of distribution functions conclude this to be a key element in reducing computational time.[23] The present program was not very sensitive to this feature. This can be attributed to the propagation of convergence technique whose application is made possible by the near linearity of the problem.

Also, the nascent electron distribution function is required as an input parameter. The nascent electrons constitute only a portion of the total electron source. The remaining source, namely the secondary electrons, is calculated within the program and is consistent with the collision rate. As before, the nascent source must be self-consistent with the other input parameters.

Finally, the convergence criterion and the number of desired iterations of the converged solution must be supplied as input parameters. The convergence criterion in conjunction with the number of simulation particles determine the accuracy of the solution and will be explained in more detail later. The parameter for the number of iterations provides a means of data smoothing. It essentially determines the number of snapshots of the distribution in time which are to be used in formulating the basis of an average. An averaging process is necessary to rid the results of fluctuations which are characteristic of all Monte Carlo simula-

tions (see Figs. 11 and 13).

2. Initialization

a. Fitting Functions of Frequently Calculated Expressions

The second section of the program contains those operations termed initialization. These operations can be divided into two types, time-saving and preliminary calculations. The distinction between them is that the preliminary calculations must precede the remaining sections of the code, whereas, the time-saving calculations are more conveniently calculated at the earlier stages of the program so that duplicate calculations may be avoided. The tabulation of integrals and the cubic-spline fitting of frequently needed, complex functions (i.e., the expression for E(t) plotted in Fig. (10)) are examples of time-saving calculations.

b. Allocation of Machine Particles

The preliminary calculations entail the distribution of the machine particles amongst the energy regions for which values of the distribution function will be calculated. The choices of average machine particle density and density distribution affect the precision of the calculated electron distribution function both globally and locally. The ideal manner in which to distribute the machine particles would be to mimic the expected electron distribution. However, the range of the variation in electron density and the fact that calculation of the extreme lower end of the distribution is unnecessary make such an approach impractical. Since the motivation of this work is to provide a basis for calculating excited state densities, the emphasis should be placed upon excitation rates, which suggests the distribution should mimic the total macroscopic excitation cross section, i.e., the range of energies where the highest

degree of accuracy is obtained contains the most particles which contribute to the excitation rate. This insures a high degree of accuracy in any calculation of excitation rates based upon the results for the distribution function obtained from this code. Due to the wide range of values of the cross section over the energy range of the calculation, these variations needed to be toned down. The distribution finally arrived at is

$$M(E) = c + \ell n \Sigma(E) \tag{71}$$

where c is a constant determined from the average error permitted and $\Sigma(E)$, the total macroscopic cross section at energy E, approximates the excitation macroscopic cross section. For 1700 machine particles, Eq. (71) yields a minimum of 50 particles per group and a maximum of 135 particles per group.

3. Convergence Propagation

The third section of the code denotes the implementation of the convergence propagation technique. The method is to take advantage of the dependence of $f(E')$ upon only $f(E > E')$, since the interaction of $f(E')$ with $f(E < E')$ is negligible compared to its interaction with the Maxwellian part of the distribution. Hence, it is inefficient to simulate the lower end of the tail of the distribution while simultaneously simulating the upper end of the tail, if the results for the upper end have not yet converged to the final solution. Thus, the calculation begins at the upper energy region until convergence is obtained, and then the simulation is expanded lower in energy, one region at a time. Such an expansion in energy is analogous to the propagation of a wave, from

one group to another, whence the name.

Convergence of a group is established by matching the flow of particles into a group with the outward flow from the group within a specified tolerance level. Care must be taken not to set the tolerance level below the noise level of the Monte Carlo simulation. The noise level is a manifestation of the fluctuations characteristic of all Monte Carlo simulations and can be approximated by the square root of the machine particle density within an energy group. If precautions are not taken and the tolerance level is set below the noise level, a superficial convergence is obtained through the compounding of random fluctuations in particle flow, producing an unphysical result.

4. Secondary Initialization

a. Initial Distribution

Appearing in the fourth section of the program is a belated initialization phase. Here, the current lowest energy group is initialized to a guess distribution. In so doing, the computational time required to obtain convergence is minimized to the degree to which the guess approximates the solution. Computational time is further reduced by introducing into an energy group $k \cdot m$ particles at m discrete energies and randomly staggering their associated times. This permits the repetitive use (k times) of the various probabilities (Eqs. (35) and (37)) necessary for the determination of the velocity of the next collision and the particle weights. The assignment of particle weights is straightforward, i.e., the number of electrons introduced into an energy interval, determined by the guess distribution, are evenly distributed over the machine particles assigned to the interval.

b. Varying Time Step Δt

The time period for which the particles are permitted to evolve is also determined in this section, permitting the period to be varied as dictated by convergence and efficiency requirements. Since the time width of an energy group (or the time for an electron to traverse an energy group) is progressively smaller for decreasing energies, the time period can be determined solely by the lowest energy group involved at any moment during the calculation. The upperbound on the time period must be less than the time width of this group in order to fully utilize the initial guess. A lowerbound is established by the graininess of the guess (or the number of discrete energies m at which the guess particles are stacked). For intermediate values, the time period is determined by requiring the number of source particles introduced into the group to be a fraction of the total number of particles within the group. Hence, we have

$$\Delta t = \begin{cases} \tau/5 & 1 < \dfrac{S(E)\tau}{f(E)} \\ \dfrac{f(E)}{5S(E)} & 2 < \dfrac{5S(E)\tau}{f(E)} < 5 \\ \tau/2 & \dfrac{5S(E)\tau}{f(E)} < 2 \end{cases} \quad (72)$$

where τ is the time width of the current lowest energy group, f(E) is the initial guess for this group, S(E) is the nascent source rate, and Δt is the calculated time period (the same Δt as in Fig. 10). The nascent source rate is used to approximate the total source rate in Eq. (72) to speed up the calculation. This is possible since only Δt, not the calculation itself, is affected.

5. Processing

a. Particle Update

In the fifth section of the program, the actual processing of particles is performed. Initially, a computational clock is incremented by the time step Δt which is calculated in the previous section of the code. Symbolically, this is representative of the next step, namely the updating process wherein all particles will be permitted to evolve for the period Δt. The evolution of the individual particles is affected as previously outlined in Section C of Chapter III, where the particle simulation is described in detail. The simulation algorithm is programmed as outlined in the flow chart in Fig. 26.

The flow chart indicates that the coding requirements to handle each of the three collisional types and hence, the costs of computation, gets progressively larger when proceeding from Coulombic interactions to excitation collisions and even larger in going to ionization events. An explanation for this trend follows. The inelastic collisions require additional coding to arrive at the electronic state in the target that will participate in the collision. The energy lost due to an excitation collision can be estimated to be the energy of excitation, thereby minimizing costs. For an ionization collision, the energy lost must be calculated by a rejection technique (subroutine EPS). Furthermore, supplemental coding is necessary in the advent of the birth of a secondary electron energetic enough to influence the calculation. This portion of the code is dominated by the time spent in calculating the energy where the secondary electron first collides. A similar calculation of the next collision energy must also be performed after the occurrence of either type of inelastic col-

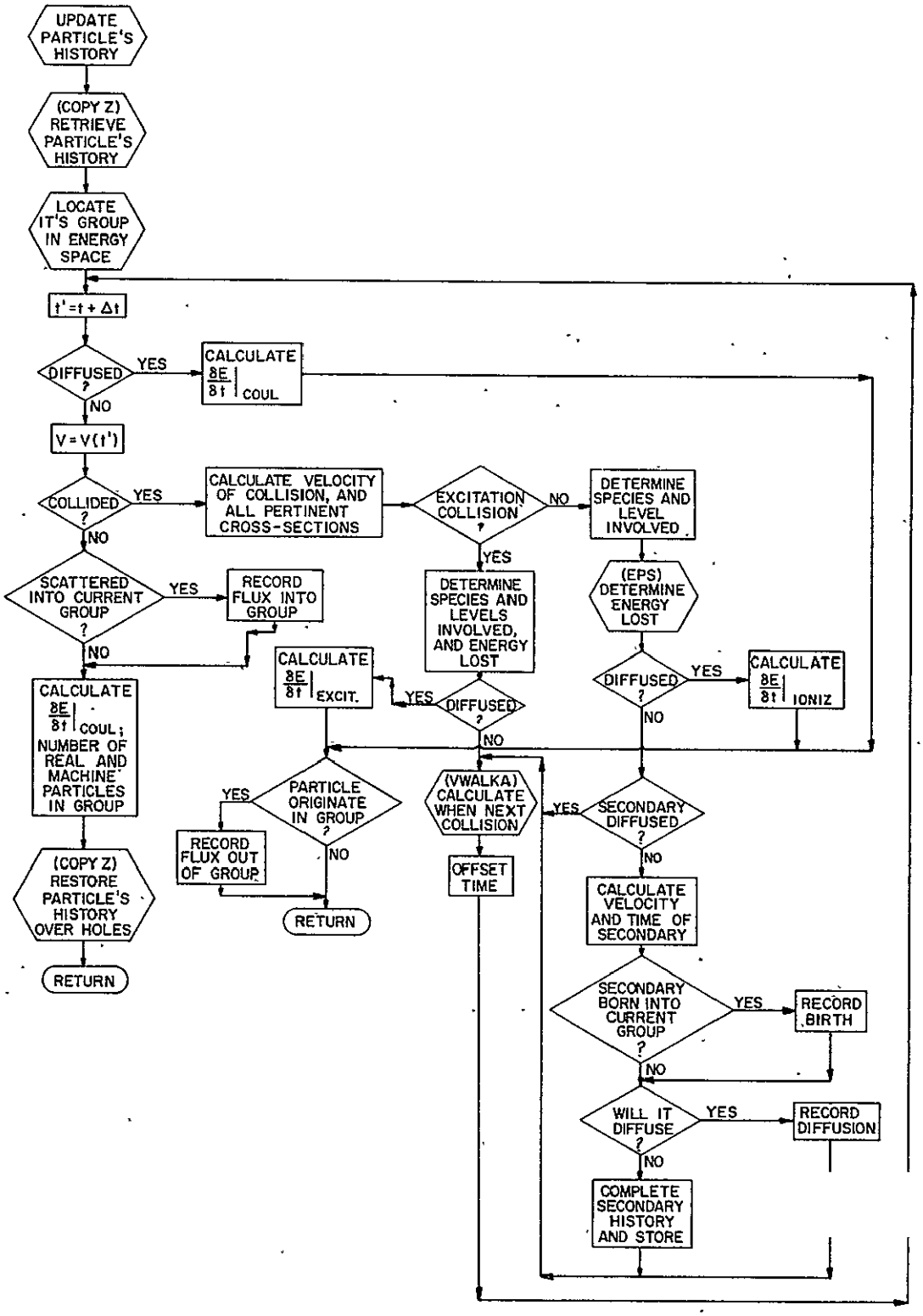

Fig. 26. Enlargement of the section of coding which updates particles.

lision. This calculation is one of the most frequently and most costly performed operations in the Monte Carlo program. The algorithm employed is a form of the rejection technique. The logic of the technique was described in Section C of Chapter III. Due to the possibility that a candidate for the collision energy may be rejected, the algorithm is a potential infinite loop (see Fig. 27). The number of circulations through the loop can be minimized by retaining one of the random number pair connected with the rejected candidate. Specifically, the random number r_2 is compared in the rejection decision process to the probability of a collision at the candidate energy determined by r_1. Then r_2 is subtracted from one and used as r_1 in the next loop. The process can be viewed in the dart analogy (see Section C of Chapter III) as reflecting the point of impact of a rejected dart from the upper right hand corner to the lower left hand corner where the dart will more likely fall below the probability distribution, resulting in the acceptance of the candidate for collision energy. The mapping of r_2 onto r_1 does not generate a true reflection. However, the collision frequencies were not altered by the above scheme. A similar scheme was also employed in the rejection technique used in calculating the energy lost due to ionization collisions with the same degree of success. Furthermore, the scheme proved to be more efficient than that used by Carter, et al.[43]

During, and after the particle has been updated, several observations are recorded pertaining to its activities. These include the initial and final location in energy space, the energy lost as well as the type of collision responsible, and the production (if any) of secondary electrons. These observations serve as the raw data for the conver-

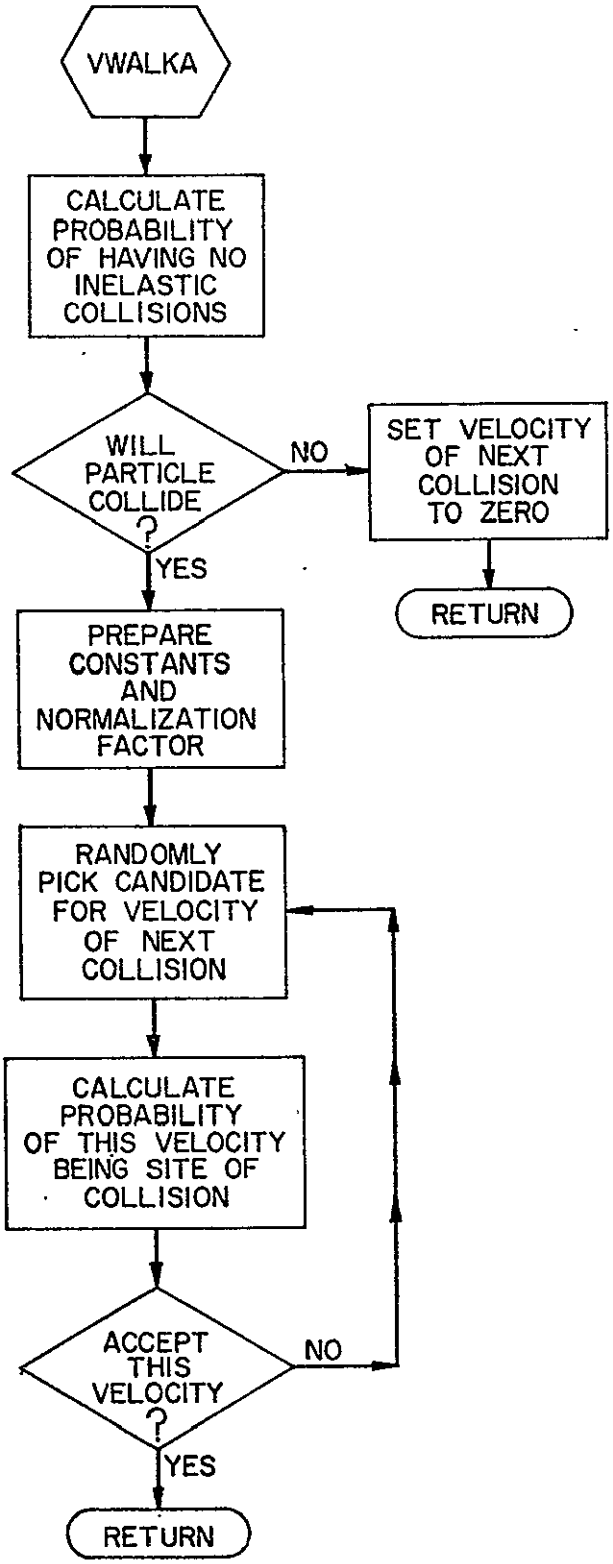

Fig. 27. Flow chart of the rejection technique employed in calculating the energy of the next collision.

gence test and the final results.

b. Secondaries

The registering of the production of a secondary electron entails the creation of a new particle with the same weight as its parent. Like its parent, it must complete its evolutionary period Δt from the time of the collision, i.e., the time $\Delta t'$ in Fig. 10. By offsetting the time of each secondary at birth by the quantity $\Delta t'-\Delta t$, the entire batch of secondaries can be updated as a group for time Δt after the original particles are processed with no distinction made in the updating process as to the particles origin. Similarly, succeeding generations of secondaries can be generated and processed, culminating in the cessation of the avalanche of secondaries.

c. Source

i. Vacancies

After secondaries are introduced into the electron population, the nascent electrons are generated as source particles. Since the machine particle population in an energy group is fixed, the injection of source particles into the particle population requires two algorithms to accommodate both vacancies and an excess of electrons in each group. Vacancies are filled with the nascent electrons in the same manner that a vacant group is initially filled with a guess distribution. However, the particle stacking procedure is complicated by the fact that the number of vacancies is not always factorable into the product of two integers k and m, where k is the number of particles to be stacked at the m discrete energies within the energy group, as was previously done. Nevertheless, the number of vacancies is resolvable as $k \cdot m + \ell$, where ℓ is also an in-

teger, thereby permitting a partial realization of the advantages of stacking particles.

ii. Excess

Should there be an excess of electrons in a group, a source particle must displace the excess particles in order to be accommodated into the group (see Fig. 28). Immediately, the question arises as to which particles in the group constitute the excess destined for extinction. This can be resolved by seeking those particles whose removal will yield the least perturbation on the calculation, i.e., those with the least weight. Once assembled, they are eliminated while retaining knowledge of the weight of the ensemble and the fraction which were to have collided. This information is combined with the weight of the source particle to be introduced and the corresponding probability of incurring a collision to generate a hybrid source particle to be added to the energy group. In this manner, none of the information retained by the "killed" particles is lost.

6. Output

In the sixth and final section of the program, the individual particle observations previously defined are accumulated for the calculation of the following quantities: flux into and out of the currently lowest energy group, secondary electron production rates, energy loss rates, the W-value (defined to be the energy lost by electrons per ion pair formed), and, of course, the distribution function corresponding to the time displayed upon the internal clock for the energy range for which convergence has been established. The particle fluxes and secondary production rates are combined with the nascent source rate to yield the

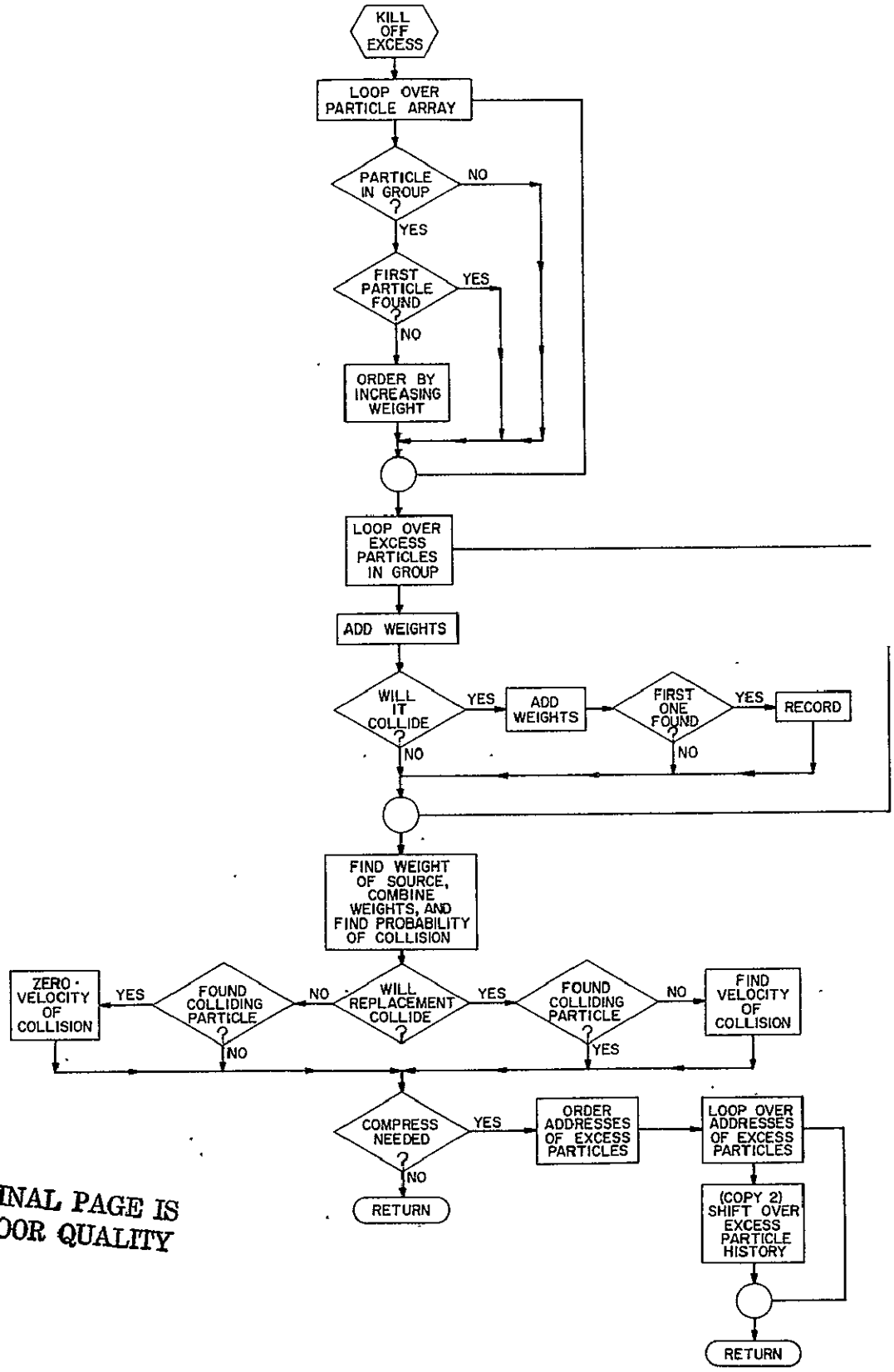

Fig. 28. Enlargement of the section of coding which kills off the excess particles in an energy group.

particle balance in energy space which serves as the convergence criterion. The particle balance, energy loss rate, and W-value are secondary output, displayed as a check upon the validity of the results and for future use.

REFERENCES

1. J. S. Kendall and T. S. Latham, "Summaries of UARL Presentations at NASA Colloqium on Uranium Plasma Research," NASA Colloqium on Uranium Plasmas, Washington, D. C., September 1973.

2. J. S. Kendall and T. S. Latham, "Summary of Fluid Mechanics and Engine Characteristics Research on the Nuclear Light Bulb Engine Concept," AIAA Paper No. 70-689, AIAA 6th Propulsion Joint Specialist Conference, San Diego, Calif., June 1970.

3. G. H. McLafferty, "Investigation of Gaseous Nuclear Rocket Technology Summary Technical Report," United Aircraft Research Laboratories report H-910093-46 (November 1969).

4. G. H. McLafferty and H. E. Bauer, "Studies of Specific Light Bulb and Open-Cycle Vortex-Stabilized Gaseous Nuclear Rocket Engines," United Aircraft Research Laboratories report F-910093-37 (September 1967). (Also issued as NASA CR-1030).

5. J. C. Guyot, G. H. Miley, J. T. Verdeyen, and T. Ganley, "On Gas Laser Pumping Via Nuclear Radiations," Symp. on Research on Uranium Plasmas and Their Technological Applications, University of Florida, 1970.

6. G. H. Miley, "Nuclear Radiation Effects on Gas Lasers," Laser Interactions, Schwarz and Hora, eds., Plenum Press, pp. 43-57 (1972).

7. G. H. Miley (ed.), "Summary of a Meeting of Non-Electrical Energy Extraction from Fusion Reactors," AEC Report COO-2218-09, Germantown, Md. (1973).

8. J. D. Clement and J. R. Williams, "Gas-Core Reactor Technology," Reactor Technology, 13, No. 3, Summer 1970.

9. N. L. Krascella, "Analytic Study of the Spectral Radiant Flux Emitted from the Fuel Region of a Nuclear Light Bulb Engine," United Aircraft Research Laboratories report J-910904-1 (1970).

10. G. H. Miley, "Direct Energy Conversion of Nuclear Energy," Am. Nuc. Soc., Hinsdale, Ill., 108ff (1971).

11. H. H. Helmick, et al., "Preliminary Study of Plasma Nuclear Reactor Feasibility," Los Alamos report LA-5679, UC-80.

12. N. L. Krascella, "Theoretical Investigation of the Spectral Opacities of Hydrogen and Nuclear Fuel," Air Force Systems Command Report RTD-TDR-63-1101 prepared by United Aircraft Research Laboratories (1963).

13. Lawrence H. Allen, Astrophysics: The Atmospheres of the Sun and Stars, The Ronald Press Co., New York (1953).

14. D. V. Sivukhin, "Coulomb Collisions in a Fully Ionized Plasma," Review of Plasma Physics, Vol. 4, Consultants Bureau, New York (1966).

15. T. Kihara and O. Aono, "Unified Theory of Relaxations in Plasmas, I. Basic Theorem," J. Phys. Soc. Japan, 18, No. 6 (1963).

16. A. Burgess and I. C. Percival, Adv. Atom. Molec. Phys., 4, p. 109-141, (1968).

17. D. E. Parks, et al., "Optical Constants of Uranium Plasmas," NASA CR-72348, N.T.I.S., Springfield, Va.

18. J. P. Shkarofsky, T. W. Johnson, and M. P. Bachynski, The Particle Kinetics of Plasmas, Addison-Wesley, Reading, Mass., 1966.

19. H. Dreicer, "Electron Velocity Distributions in a Partially Ionized Gas," Phys. Rev., 117, 343 (1960).

20. D. C. Montgomery and D. A. Tidman, Plasma Kinetic Theory, McGraw-Hill Book Co., New York (1964).

21. N. A. Krall and A. W. Trivelpiece, Principles of Plasma Physics, McGraw-Hill Book Co., New York (1973).

22. R. Lo, "Energy Distributions of Electrons in Radiation Induced-Helium Plasmas," Ph.D. Thesis, Nuclear Engineering Program, Univ. of Illinois, Urbana, Ill. (1972).

23. B. S. Wang and G. H. Miley, "Monte Carlo Simulation of Radiation-Induced Plasmas," Nucl. Sci. Eng., 52, 130-134 (1973).

24. M. N. Rosenbluth, W. M. MacDonald, and D. L. Judd, "Fokker-Planck Equation for an Inverse-Square Force," Phys. Rev., 107, No. 1, p. 1 (1957).

25. W. L. Nighen, "Electron Energy Distributions and Collision Rates in Electrically Excited N_2, CO and CO_2," Phys. Rev., 2A, 1989 (1970).

26. T. Holstein, "Energy Distribution of Electrons in High Frequency Gas Discharges," Phys. Rev., 70, p. 367 (1946).

27. U. Fano, "Degradation and Range Staggling of High-Energy Radiation," Phys. Rev., 92, 328 (1953).

28. L. V. Spencer and U. Fano, "Energy Spectrum Resulting from Electron Slowing Down," Phys. Rev., 93, 1172 (1954).

29. W. E. Wells, P. Monchicourt, R. Deloche, and J. Berlande, "Theoretical Computations of the Effects of the Metastable Populations on Electron Energy Balance and Distribution Function in a Helium Afterglow," Phys. Rev., 8A, 381 (1973).

30. R. W. L. Thomas and W. R. L. Thomas, "Monte Carlo Simulation of Electrical Discharge in Gases," J. Phys. B (At. Molec. Phys.) Ser. 2, 2, 562 (1969).

31. G. Safonov, R. Witte, S. Altschuler, and W. Simmons, "An Experiment for Pursuit of the Fission Laser," Rand Report, unpublished internal report, TRW Corporation, El Segundo, Calif., July 1971.

32. U. Fano and L. V. Spencer, "Quasi-Scaling of Electron Degradation Spectra," submitted to International J. Rad. Phys. and Chem.

33. R. W. Bussard and R. D. DeLauer, Nuclear Rocket Propulsion, McGraw-Hill Book Co., Inc., 160, New York (1958).

34. J. Spanier and E. M. Gelbard, Monte Carlo Principles and Neutron Transport Problems, Addison-Wesley Publishing Co., Reading, Mass., 26ff (1969).

35. A. Lenard, "On Bogolinbov's Kinetic Equation for a Spatially Homogeneous Plasma," Ann. Phys. 10, 390 (1960).

36. J. Hubbard, "The Friction and Diffusion Coefficients of the Fokker-Planck Equation in a Plasma, II," Proc. Roy. Soc. A 261, 371 (1961).

37. Y. Itikawa and O. Aono, "Energy Change of a Charged Particle Moving in a Plasma, Phys. Fluids, 9, 1259 (1966).

38. Private communication with Y. Itikawa.

39. F. Perkins, "Motion of a Test Particle in a Plasma," Phys. Fluids, 8, 1361 (1965).

40. S. T. Butler and M. J. Buckingham, "Energy Loss of a Fast Ion in a Plasma," Phys. Rev., 126, 1 (1962).

41. L. J. Kieffer, "A Compilation of Electron Collision Cross-Section Data for Modeling Gas Discharge Lasers," J.I.L.A., Information Center Report 13, University of Colorado, Boulder, Colorado, Sept. 1973.

42. Sanborn C. Brown, Basic Data of Plasma Physics, The M.I.T. Press, Cambridge, Mass. (1966).

43. L. L. Carter, E. D. Cashwell, and W. M. Taylor, "Monte Carlo Sampling with Continuously Varying Cross Sections Along Flight Paths," Nuc. Sci. Eng., 48, 403-411 (1972).

44. J. R. Lamarsh, Introduction to Nuclear Reactor Theory, Addison-Wesley Publishing Company, Inc., Reading, Mass., 187ff (1966).

45. D. Suhre, Ph.D. Thesis, Electrical Engineering Department, Univ. of Illinois, Urbana, Illinois (1975).

46. U. Daybelge, "Unified Transport Theory of Partially Ionized Non-isothermal Plasmas," J. Applied Physics, 41, 2130 (1970).

47. D. J. Sigmar and G. Joyce, "Plasma Heating by Energetic Particles," Nuclear Fusion 11, 447 (1971).

VITA

Charles Gary Bathke was born in [redacted] on [redacted]. He received the B.S. degree in Physics from the Ohio State University at Columbus in 1970. He then enrolled at the University of Illinois at Urbana-Champaign in the Department of Physics where he held a position as a teaching assistant for two years. Upon receiving the M.S. degree in Physics in 1972, he transferred to the Nuclear Engineering Program at the University of Illinois where he became a research assistant.

As a Ph.D. candidate in the Nuclear Engineering Program, he co-authored a number of papers relating to both fusion and uranium plasmas which appeared in such journals as the ANS Transactions. In 1974, he received the Best Student Contributed Paper Award, Isotopes and Radiation Division for a paper presented at the 1974 Winter Meeting of the American Nuclear Society. He is also a member of the American Nuclear Society.